Hindawi
Geofluids
Volume 2019, Article ID 6727681, 21 pages
https://doi.org/10.1155/2019/6727681

Research Article

Applying Rare Earth Elements, Uranium, and $^{87}Sr/^{86}Sr$ to Disentangle Structurally Forced Confluence of Regional Groundwater Resources: The Case of the Lower Yarmouk Gorge

Christian Siebert,[1] Peter Möller,[2] Fabien Magri,[3,4] Eyal Shalev,[5] Eliahu Rosenthal,[6] Marwan Al-Raggad,[7] and Tino Rödiger[8]

[1]*Dept. of Catchment Hydrology, Helmholtz Centre for Environmental Research (UFZ), Halle/Saale, Germany*
[2]*Helmholtz Centre Potsdam, German Research Centre for Geosciences (GFZ), Section 3.4, Potsdam, Germany*
[3]*Dept. of FA 2, Federal Office for the Safety of Nuclear Waste Management (BfE), Berlin, Germany*
[4]*Hydrogeology, Freie Universität, Berlin, Germany*
[5]*Geological Survey of Israel (GSI), Jerusalem, Israel*
[6]*The School of Earth Sciences, Tel Aviv University, Tel Aviv, Israel*
[7]*The Inter-Islamic Network on Water Resources Development and Management (NWRDAM), Amman, Jordan*
[8]*Dept. of Computational Hydrosystems, Helmholtz Centre for Environmental Research (UFZ), Leipzig, Germany*

Correspondence should be addressed to Christian Siebert; christian.siebert@ufz.de

Received 24 May 2019; Revised 23 September 2019; Accepted 3 October 2019; Published 3 December 2019

Guest Editor: Tanguy Robert

The conjoint discussion of tectonic features, correlations of element concentrations, $\delta^{18}O$, δD, and $^{87}Sr/^{86}Sr$ of groundwater leads to new insight into sources of groundwater, their flow patterns, and salinization in the Yarmouk Basin. The sources of groundwater are precipitation infiltrating into basaltic rock or limestone aquifers. Leaching of relic brines and dissolution of gypsum and calcite from the limestone host rocks generate enhanced salinity in groundwater in different degrees. High U(VI) suggests leaching of U from phosphorite-rich Upper Cretaceous B2 formation. Both very low U(VI) and specific rare earth element including yttrium (REY) distribution patterns indicate interaction with ferric oxyhydroxides formed during weathering of widespread alkali olivine basalts in the catchment area. REY patterns of groundwater generated in basaltic aquifers are modified by interaction with underlying limestones. Repeated sampling over 18 years revealed that the flow paths towards certain wells of groundwater varied as documented by changes in concentrations of dissolved species and REY patterns and U(VI) contents. In the Yarmouk Gorge, groundwater with basaltic REY patterns but high U(VI) and low Sr^{2+} and intermediate sulfate concentrations mainly ascends in artesian wells tapping a buried flower structure fault system crossing the trend of the gorge.

1. Introduction

Since Roman times, the hot springs of Hamat Gader (HG), Israel, and Ain Himma, Jordan, in the Lower Yarmouk Gorge (LYG) were used for health care (Figure 1). At present, only Ein Balsam at HG is publically in use. Hydrogeological and hydrochemical studies of springs and well waters in the gorge reveal that groundwater of widely different composition discharges at short distances [1]. By major and minor elements and distribution patterns of rare earth elements including yttrium (henceforth termed REY), it was ascertained that thermal groundwater discharging through springs in the LYG is infiltrated in basaltic regions of the Hauran plateau, Syria [1]. Parts of these waters are mixed in various proportions with limestone water from Ajloun. The hot waters of Hamat Gader and Meizar get salinized by either mixing with relic seawater evaporation brines [2, 3] or leaching of evaporites. The recent study is based on 18 years of repeated sampling of wells and springs and reveals significant variations in REY patterns and element concentrations suggesting

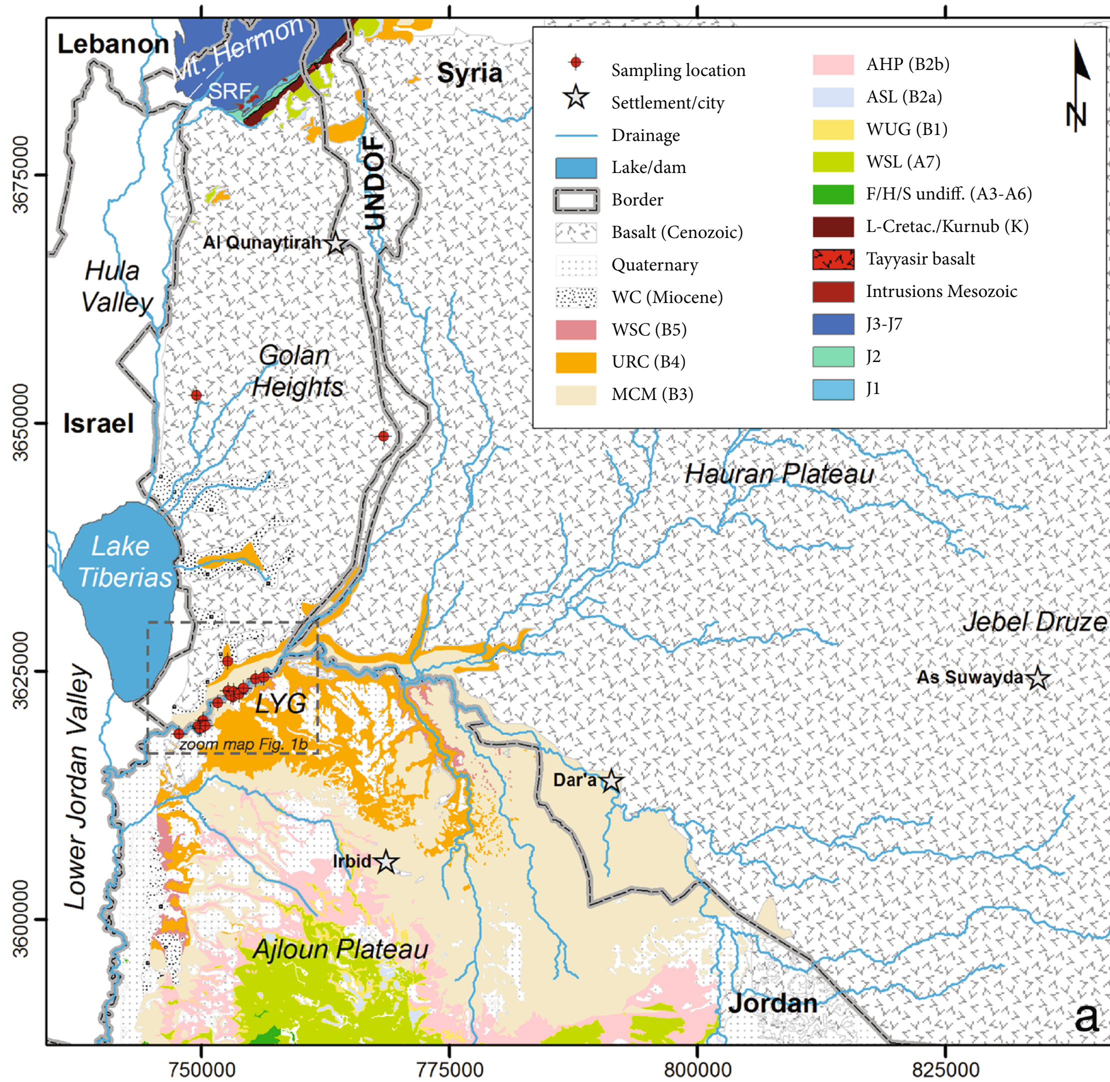

Sampling location	X (UTM)	Y (UTM)	Short
Groundwater wells			
Mukheibeh 1	753119	3622154	M1
Mukheibeh 2	753241	3622342	M2
Mukheibeh 4	753212	3622331	M4
Mukheibeh 5	747753	3618570	M5
Mukheibeh 6	753018	3622417	M6
Mukheibeh 7	754257	3623142	M7
Mukheibeh 8	755495	3624134	M8
Mukheibeh 9	756312	3624296	M9
Mukheibeh 10	753267	3622856	M10
Mukheibeh 11	753845	3622588	M11
Mukheibeh 13	754268	3623212	M13
Meizer 1	752652	3625884	Me1
Meizer 2	752706	3622894	Me2
Meizer 3	752725	3622926	Me2
Spring (Hamat Gader)			
Ein Balsam	749705	3619324	EB
Ein Makla	749859	3619141	EM
Ein Reach	750014	3619198	EB
Ein Sahina	750190	3619926	EB
Ain Saraya	750429	3619424	EB
Spring (Himma)			
Ain Himma	751661	3621700	AH
Spring (Golan Hieghts)			
Umm Abu ad Danar	763884	3648639	
Amphy spring	748804	3653081	
River			
Yarmouk River	756255	3624301	YR

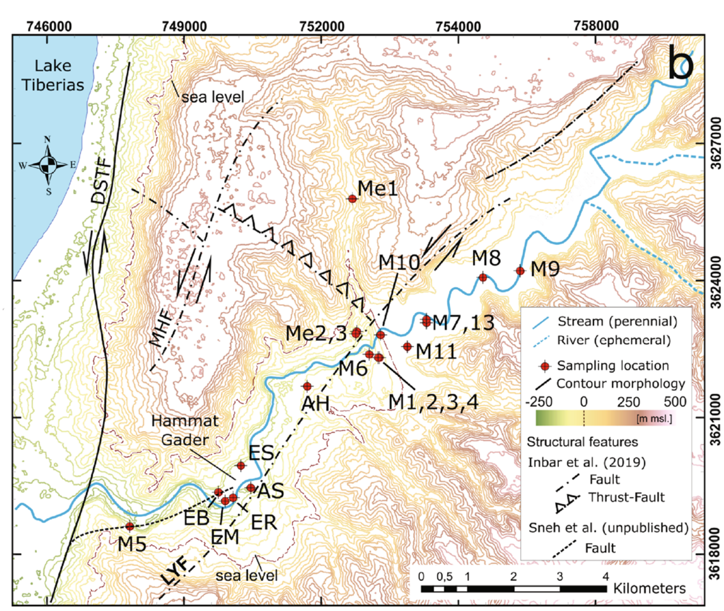

Figure 1: Overview of the study area, showing geological background (a) and sampling locations (b) including structural features recently introduced by Inbar et al. [15] and Sneh (unpublished).

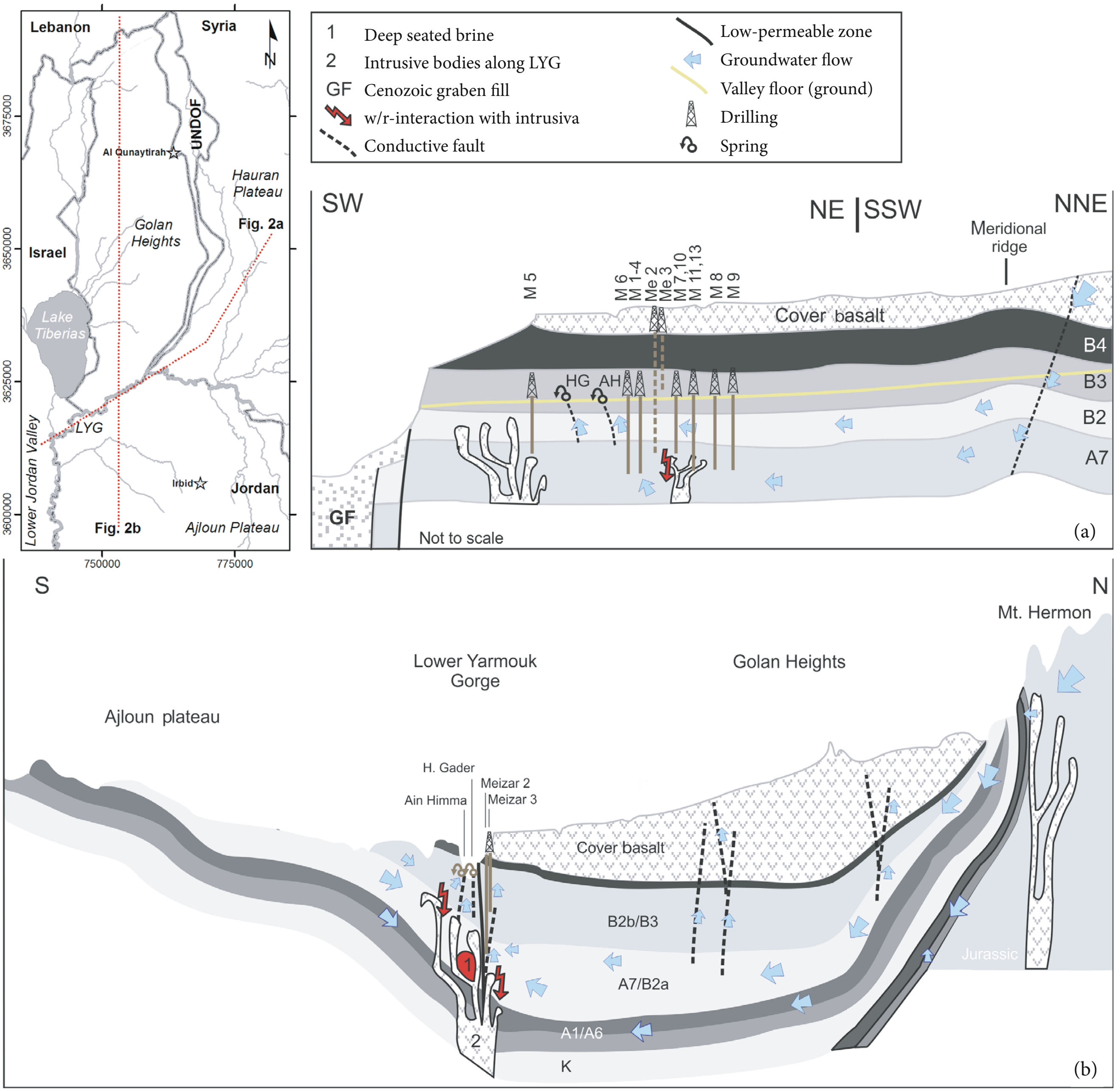

FIGURE 2: Schematic geological cross sections (not to scale). Section (a) starts in the Lower Jordan Valley, continues through the LYG, and branches into the Hauran NE-ward, while section (b) cuts from the Ajloun northward across the LYG and the Golan Heights into Mt. Hermon. The map shows the location of cross sections in red.

variation of flow paths and associated interactions with host rocks and leaching residual brines and evaporites.

The chemical and isotopic composition of the large amounts of fresh artesian groundwater produced in the Jordanian Mukheibeh well field contrasts with that of the saline groundwater in the Meizar wells and the springs of Hamat Gader. This gave rise to the conceptual model that the LYG is the surface expression of a fault zone, preventing transboundary flow [1]. 2D and 3D modelling supported that concept of continuous groundwater aquifers with the absence of transboundary groundwater exchange due to a zone of high hydraulic anisotropy underneath the gorge's centerline [4–7]. The gorge seemingly acts as a complex conduit-barrier system, along which groundwater from the Golan in the north and Ajloun in the south converges and drains towards the Lower Jordan Valley (Figure 2). Flow paths in the underground of the gorge possibly occur along faults oriented perpendicular to the major axis of the gorge [5, 6, 8].

Based on stratigraphic data [9, 10], topographic data, deep seismic survey data [11, 12], shallow fault mapping [13], and thickness irregularities of the Turonian and Senonian sequences in the study area [14–17] support the occurrence of strike-slip flower structure faults along and across the gorge creating a series of structural fault blocks and numerous buried faults at close proximity to the Dead Sea Transform Fault (DSTF) (Figure 1).

Applying REY distribution patterns, U(VI), $^{87}Sr/^{86}Sr$, and water isotopes in a new, complete, and synchronous set of sampled spring and well waters in 2016, we aim for joint discussion of hydrochemical and geological features to improve the knowledge of the sources of groundwater and of their flow paths.

After the introduction (Section 1), we will present the hydrogeological setting of the studied area (Section 2), the sample acquisition and the techniques used to analyze them (Section 3), the results on major and minor element, particularly on REY and U(VI), and Sr isotopes (Section 4), and a detailed discussion (Section 5). Section 6 concludes this study.

2. Hydrogeological Setting

Geographically, the Yarmouk drainage basin comprises (i) the volcanic Hauran plateau and the western flank of the Jebel Druze volcano [18], (ii) the southern and southeastern slopes of Hermon, (iii) the Golan Heights with numerous volcanic cones, (iv) the northern plunges of the Ajloun anticline, and (v) the Azraq-Dhuleil basin ENE of Ajloun (Figure 1(a)).

The Mediterranean climate in the Yarmouk basin causes rainy and cool winters and hot and dry summers. The distinct differences in altitude and the distance from the Mediterranean force strong gradients in annual precipitation. Highest values (up to 1300 mm/a) fall in the Hermon Massif and the highest parts of Jebel Druze; medium elevated regions such as the Hauran and Ajloun plateaus and the Golan Heights receive 600-800 mm/a, while the low-lying LYG and the xeric region SE of the surface drainage basin receive <500 mm/a only (e.g., [18–21]). The resulting recharge fractions are calculated to range from 0.06 to 0.1 [20, 22–24].

In the south of the Yarmouk River, geological formations dip NW-ward (Figure 2). Here, the oldest hydrogeological relevant formations comprise the highly karstified lime- and dolostones of the Upper Cretaceous A7 aquifer and the overlaying heavily fractured silicified limestones of the Eocene B2 aquifer, altogether forming the 160 m thick regional A7/B2 aquifer system (Figure 3). This system becomes efficiently confined due to its descent and the appearance of the covering B3 aquiclude. On top of the southern flank of the LYG, remnants of the B4 sequence form a local limestone aquifer.

All formations older than B4 continue in the underground of the Golan Heights syncline before they partly resurface in the foothills of the Hermon anticline [25]. Underneath the Golan Heights, Jurassic limestones form the base of the formations before they become uplifted in the Hermon anticline in the north (Figures 1(a) and 2(b)). Since the drainage basin extends into three nations with different geological terminologies. Figure 3 compiles the relevant parts of the stratigraphic columns for the entire region.

Morphologically, the Golan Heights is restricted southward by the LYG, westward by the Hula Valley and Lake Tiberias, northward by Wadi Sa'ar at the foothills of Mt. Hermon, and eastward by Wadi Raqqad. The entire Golan Heights is unconformably overlain by Plio-Pleistocene cover basalts, which continue E- and SE-ward into the Hauran plateau, Jebel Druze, and Azraq-Dhuleil Basin and form the uppermost supraregional aquifer in the area [26, 27]. Within the Golan Heights, the thickness of the basalts varies with more than 750 m in the central part and less than 50 m along the LYG (Figure 2(b)) and B3 layers form the impervious base of the basaltic aquifer [28–30]. However, the basaltic aquifer is connected to underlying aquifers at certain locations [31], either where B3 was already eroded or where structurally prominent features of post-Pliocene age cut the formations [12, 28, 32, 33]. An aeromagnetic survey in N Jordan revealed a SW-NE lineament branching from the DSTF towards Hamat Gader in the LYG [34], which was later proven to be a fault by geological mapping (Sneh et al., unpublished) (Figure 1(b)).

The groundwater in the phreatic and shallow basaltic aquifer mainly follows the morphology. Within the Golan Heights, it flows W- and SW-ward towards the Hula Valley, the Lake Tiberias, and the LYG [28, 33]. In the east, a subterranean meridional ridge forms a water divide against the Hauran [19] (Figure 2(a)). The thin lava flows east of the water divide, hosts only modest amounts of groundwater, and discharges locally into incised wadis, e.g., the Raqqad. The basaltic cover of the Hauran plateau is mainly recharged at the elevated southeastern flanks of the Hermon Massif and western piedmont of Jebel Druze, from where the groundwater flows SE- and W-ward, respectively. The groundwater most probably converges in the central part of the Hauran and flows from there SW-ward towards the LYG. There, the observed groundwater of this study discharges either naturally at the valley floor through springs in Hamat Gader, Suraya, and Himma or artificially through the (mostly) artesian wells of Mukheibeh and Meizar, located in the flanks of the gorge, either north (Meizar wells) or south (Mukheibeh wells) (Figure 1(b)).

3. Analytical Procedures

The elements Ca^{2+}, Mg^{2+}, U(VI), and REY are determined by ICP-MS (Elan DRC-e). K^+ and Na^+ were analyzed by ICP-AES (Spectro Arcos) using matrix-adjusted standard solution for calibration. Cl^-, Br^-, and SO_4^{2-} are determined with Dionex ICS (AS18 column). The alkalinity is titrated to pH 4.3 with H_2SO_4 and given as HCO_3^-.

To determine REY and U(VI), preconcentration is required. Therefore, about 4 l of sample is filtered in the field by using a peristaltic pump coupled to 0.2 μm filters (Sartorius, Germany). The samples are acidified by subboiled (index sbb) HCl, and 1 ml of Tm spike solution is added. At the same day, the samples are adjusted to pH = 2 using HCl_{sbb} and subsequently passed through preconditioned C_{18} Sep-Pak cartridges (Waters, USA), loaded with an ethylhexyl phosphate (Merck, Germany) liquid ion exchanger, at a rate of 1 l/h. Thereafter, each cartridge is washed with 50 ml of 0.01 M HCl_{sbb} and subsequently eluted with 40 ml of 6 M HCl_{sbb} at a rate of 3 ml/min. The eluates are evaporated to incipient dryness, and the residues are dissolved in 1 ml of

System	Age	Group			Formation			Hydrogeological properties			
	Period	GH/Mt.H	Ajloun	DB/H	GH/Mt.H	Ajloun	DB/H	Golan/Mt. Hermon	Ajloun		Damascus Basin/Hauran
Quaternary	Quaternary				Yarmouk Basalt			Alkaline-olivine basalt	Alkaline-olivine basalt	Plateau Basalts	Gravel, gipseous marl, siltite, clay
Neogene	Pliocene	Kefar Giladi		Jeribe Chilou	Cover basalt		n3				Sandstone, siltite
					Bira/Gesher				Silicified limest., dolomite		Alternation congl., marl, limest.
	Miocene				Hordos	Waqqas conglomerate (WC) - Jordan Valley	n2	Conglomerates in siltand clay matrice	Marl, sand		Limestone
					Lower basalt				Alkali olivine basalt		Conglomerates in limy matrix
Paleogene	Oligocene				Susita/Fiq		n1		Marlst., sandy dolomite		Marl, clay, conglomerates
	Eocene		Belqa	Jaddala		Wadi Shallalah chalk (WSC) (B5)	e5		Chalk, bituminous		Thick banked limestone, upper part chalky, marly
		Avedat			Maresha/ Adulam	Umm Rijam (URC) (B4)	e4	Marl, chalk, limestone	chalky limest., chert beds		Massive limestone
	Upper Maastricht-Paleocene	Mt. Scopus		Kermev Bardeh	Taqiye	Muwaqqar chalk (MCM) (B3)	e1-e3	Marly limestone, bituminous, chert, phosphorite	Micritic limest., bituminous (oil shale)		Alternating chak, marl
Cretaceous	Masstrichtian			Soukhne	Ghareb	Al Hasa phosphorite (AHP) (B2-b)	m1, m2		Calcareous, phosphorite beds, limest., chalk, marl		Alternating chalk, marl, limest., cherts
	Campanian				Mishash	Amman silicified limestone (ASL) (B2a)	S		Limestone., dolomite, chalky, phosphate, chert		Chalk, marl
	Santonian				Menuha	Wadi Umm Ghudran (WUG) (B1)			Massive chalk, limest., phosphatic sandst., chert		
	Turonian	Judea	Ajloun	Judea	Bina	Wadi Es Sir Limest. (WSL) (A7)	t2	Limestone, dolomite, marly limest.	Dolomitic limest., sandst., cherts		Banked limestone
	Cenomanian-Turonian					F/H/S-undifferentiated	t1		Marl and gypsum		
						Shueib (S) (A5-6)			Siltstone, marly limest., dolomite		
	Cenomanian				Saknin	Hummar (H) (A4)	c	Dolomitic limestone	Dolomitic limestone, karstic limestone		Banked limestone, partly dolomite
								Karstic limest., chert			
		Kurnub			Deir Hanna	Fuheis (F) (A3)		Chalk beds, thin dolost.	Calcareous siltst., marly lime-/ dolost., chalk beds		
						Na'ur (NL) (A1-2)			Glauconitic sandstone		
									Limest., dolomite		
	Albian		Kurnub		Yagur	Subeihi (K2)	ab	Dolomite, limestone	Sandstone		Marly limestone
	Aptian				Yakhini		a1-a3	Sandstone			
					Banias, Tayassir basalt			Basalts			Clayey sandstone, limestone intercalated
	Barremian										
	Hauterivian-Berriasian					Aarda (K1)					
Jurassic	Malm	Arad	Zarqa		J6-J7 (Nahal Saar)	Azab	j5-j7	Limestone	Sandstone, siltstone, limestones	basalts	Limestone
					J5 (Kidod)			Marl, shale			Marl
	Dogger				J4 (Hermon/ Zohar)		j2-j4	Limestone			Dolomitic limestone at base, limestone on top
	Lias				J1-J3		j1	Dolomite, limestone			Marl lignite, dolomite, sand- and limestone

GH = Golan Heights, Mt.H = Mount Hermon, DB = Damascus Basin, H = Hauran; Syrian geology taken from Brew et al. [26] and Wolfart [27]

Figure 3: Stratigraphic table of the hydrogeological formation in the Yarmouk Basin.

5 M $HNO_{3\ sbb}$ (Merck, Germany) and transferred into 10 ml volumetric flasks. 1 ml of spike solution is added which is used, if necessary, for drift corrections of the response factors during the ICP-MS measurements.

Stable isotopes of oxygen and hydrogen are determined in separate filtered samples (0.2 μm) using laser cavity ring-down spectroscopy (Picarro L2120-i, USA) without further treatment of the water samples. The respective analytical precision is ±0.1‰ and ±0.8‰ for $\delta^{18}O$ and δD, respectively. The results are reported relative to Vienna Standard Mean Ocean Water (VSMOW).

Analyses of $^{87}Sr/^{86}Sr$ in water samples were performed at TUBAF, Freiberg, Germany. Samples were prepared and analyzed after Tichomirova et al. [35] by applying TIMS (Finnigan MAT 262) with an acceptable relative error of ±0.005% for $^{87}Sr/^{86}Sr$. Sr-isotope ratios are given in respect to NBS-987. To analyze Sr^{2+} in basaltic rock samples, rocks have been powdered to <150 μm, pressed to pellets, and analyzed applying energy-dispersive X-ray fluorescence (EDXRF) (Spectro XEPOS HE 2000). Chemical and isotopic analyses are given in Tables 1–3.

4. Results

Depending on the sampling location, the results are classified in the following way: Mukheibeh well field (M1-M13), Ain Himma (AH), Hamat Gader springs (HG), Meizar wells (Me1-Me3), and the Yarmouk River (YR). Sampling locations, which have been repeatedly sampled, are indicated by the year of sampling given in parentheses. The Hebrew and Arabic term of springs is transliterated as Ein and Ain, respectively.

4.1. Major and Minor Element Correlations with Cl^-. From the low-salinity Mukheibeh clusters, two (Figures 4(a)–4(f)) or one (Figures 4(g)–4(j)) mixing lines evolve with high-salinity end members. They indicate that two end member brines occur in the study area: one is salinizing the Meizar wells and Ain Himma and the other the springs of Hamat Gader (Ein Maqla, Ein Reach, Ein Balsam, and Ain Sarayah). The Ca^{2+} concentration in Ain Himma switches between the two trends, probably because the access point to sample the spring water within the increasingly ruined Himma resort

Table 1: Compilation of groundwater analyses from the Lower Yarmouk Gorge and surrounding areas.

ID	Source	Abbr.	X	Y	Sampling Date	pH	Eh mV	Temp °C	EC μS/cm	Alk	Ca mg/l	Mg mg/l	K mg/l	Sr mg/l	Na mg/l	Cl mg/l	SO_4 mg/l	Br mg/l	HCO_3 mg/l	U nmol/l	$\delta^{18}O$ VSMOW	δ^2H VSMOW
Groundwater wells																						
01-128	Mukheibeh 1	M1 (01)	753119	3622154	#######	7	67	29.1	797	5.93	91.3	30	3.1	0.69	39	57.2	54.3	0.20	358	105.2	-5.65	-27.40
13/803	Mukheibeh 2	M2 (13)	753243	3622340	#######	7.12	65	28.14	809	5.18	96	30	3.02	0.54	38.7	58.4	57.2	0.09	312	88.2	-5.64	-26.40
16/08	Mukheibeh 2	M2 (16)	753241	3622342	#######	6.13	18	28.9	830	4.56	78	26	2.9	0.51	39	56.4	56.1	0.1	274	88.2	-5.38	-25.51
13/802	Mukheibeh 4	M4 (13)	753209	3622333	#######	7.1	63	28.8	807	5.18	96	29	3	0.51	38.5	55.4	54.7	0	312	96.6	-5.26	-25.40
16/09	Mukheibeh 4	M4 (16)	753212	3622331	#######	7.04	273	29.1	827	4.76	84	28	2.9	0.5	40	56.5	57.1	0.09	286	92.4	-5.50	-25.47
16/12	Mukheibeh 5	M5 (16)	747753	3618570	#######	7.32	162	40.9	876	5.08	71	24	3.8	0.94	47	57.2	36.3	0.11	305	4.6	-5.16	-24.54
16/10	Mukheibeh 6	M6 (16)	753018	3622417	#######	7.06	-40	31	667	5.08	86	29	3.4	0.66	49	73.3	59.8	0.26	306	58.8	-5.43	-26.28
16/14	Mukheibeh 7	M7 (16)	754257	3623142	#######	7.17	-17	38.5	774	4.8	84	29	2.9	0.54	40	60.5	35.5		288	63.0	-5.58	-27.04
13/804	Mukheibeh 8	M8 (13)	755490	3624127	#######	7.45	-123	44.9	701	4.72	68	20	5.25	1.4	53.3	64.5	27.8	0.12	283	0.0462	-6.28	-30.99
16/16	Mukheibeh 8	M8 (16)	755495	3624134	#######	7.16	-62	44.9	723	4.1	59	20	5.1	1.3	56	66.6	12.7	5.55	246		-6.09	-30.01
16/17	Mukheibeh 9	M9 (16)	756312	3624296	#######	7.2	-67	28.9	1157	7.6	54	29	16	5.3	120	82.6	21	0.19	459		-6.54	-32.16
16/11	Mukheibeh 10	M10 (16)	753267	3622856	#######	6.96	-117	39	710	4.34	72	25	3.7	0.96	47	59.9	39.5		261	5.0	-5.67	-27.37
16/13	Mukheibeh 11	M11 (16)	753845	3622588	#######	6.92	200	31.9	821	4.8	76	39	2.8	0.87	44	56.4	53.3	0.09	289		-5.34	-25.75
13/805	Mukheibeh 13	M13 (13)	754280	3623202	#######	7.38	-76	38.5	752	5.12	81	25	3.74	0.94	43.6	59.1	24.5	0.1	307	3.7	-5.69	-27.78
16/15	Mukheibeh 13	M13 (16)	754268	3623212	#######	7.12	-47	38.9	778	4.4	72	25	3.7	0.88	46	61.7	34		264	8.0	-5.65	-27.04
16/07	Meizar 1	Me1	752652	3625884	#######	7.38	-79	35.2	1630	3.64	52	17	13	2.1	230	386	12.7	2.39	217		-5.98	-29.13
01-166	Meizar 2	Me2 (01)	752700	3622914	#######	6.63	-102	60	1650	4.06	142	34.8	21.8	5.16	178	317	278	3.90	244	0.059	-5.90	-29.40
08/753	Meizar 2	Me2 (08)	752715	3622884	#######	6.75	-106	57.1	2060	3.76	178	42.1	24.6	5.8	201	373	328	4.44	225	0.063	-6.87	-36.61
16/02	Meizar 2	Me2 (16)	752706	3622894	#######	6.4	-77	60.6	2080	3.68	170	37	24	5.5	210	392	338	3.6	221		-6.89	-35.25
01-167	Meizar 3	Me3 (01)	752707	3622923	#######	7.09	-129	41.8	664	5.24	65.3	20.9	4.7	1.25	48.5	61.6	4	0.20	315	0.045	-6.84	-33.00
08/752	Meizar 3	Me3 (08)	752721	3622900	#######	6.6	-117	57.4	2090	3.72	177	42.2	24.2	5.8	200	365	306	3.97	223	0.078	-6.87	-36.61
16/01	Meizar 3	Me3 (16)	752725	3622926	#######	6.81	-120	42.2	810	5.48	71	25	3.9	1.1	53	78.7	19.3	0.35	330		-5.85	-28.29
Springs (Hamat Gader fresh)																						
16/03	Ein Sahina	ES	750190	3619926	#######	7.04	454	28	844	5	87	28	3.3	0.56	44	66.5	48.9	0.2	301	19.3	-5.57	-26.13
Springs (Hamat Gader thermohaline, incl. Ain Saraya)																						
16/04	Ein Balsam	EB	749705	3619324	#######	6.76	11	41.9	1600	4.8	120	34	12	3.5	130	325	133	2.92	289	4.6	-5.84	-28.53
00-107	Ein Reach	ER (00)	750349	3619399	#######	6.85	-96	38	1728	6	142	39.5	12.2	2.94	143	309	115	3.82	362	9.1	-5.84	-29.90
04-585	Ein Reach	ER (04)	749985	3618816	#######	6.81	-147	41.5	1759	5.86	134	39.5	12.6	3.44	156	345	119	4.25	353	7.9	-5.99	-29.90
16/05	Ein Reach	ER (16)	750014	3619198	#######	6.69	-76	43.4	1860	4.84	130	37	14	4.2	160	376	128	3.37	291	7.6	-5.93	-28.59
00-108	Ein Makla	EM (00)	749909	3619091	#######	6.64	-131	47.3	2190	5.64	178	44.2	18	5.21	212	488	158	6.55	340	5.8	-6.00	-31.60
04-586	Ein Makla	EM (04)	749811	3618793	#######	6.73	-167	49.6	2160	5.42	152	42	17.2	5.19	209	465	151	5.98	327	5.7	-6.15	-31.30
16/06	Ein Makla	EM (16)	749859	3619141	#######	6.59	-116	49.5	2160	3.64	150	39	17	5.5	210	475	150	4.51	218	5.9	-6.08	-29.59
16/20	Ain Saraya	AS	750429	3619424	#######	6.83	-16	38.3	1655	4.54	130	38	12	3.8	160	342	120	3.02	273	8.0	-5.85	-28.56

Table 1: Continued.

ID	Source	Abbr.	*X*	*Y*	Sampling Date	pH	Eh mV	Temp °C	EC μS/cm	Alk	Ca mg/l	Mg mg/l	K mg/l	Sr mg/l	Na mg/l	Cl mg/l	SO_4 mg/l	Br mg/l	HCO_3 mg/l	U nmol/l	$\delta^{18}O$ VSMOW	δ^2H VSMOW
Springs (Himma thermohaline)																						
01-12	Ein Himma	AH (01)	751665	3621722	#######	7.06	-145	41.5	1418	5.59	108	34.9	13.9	2.88	124	208	148	2.25	337	4.1	-6.08	-32.00
07/624	Ein Himma	AH (07)	751665	3621722	#######	7.02	-28	40	1433		113	34	13.8	3.7	122	244	212	2.9	330	2.3	-6.16	-31.13
11/140	Ein Himma	AH (11)	751568	3621767	#######	7.11	492	27.5	1071	5.56	105	34.5	8.7		82.3	143	124	0.97	335	9.3	-5.29	-23.86
13/807	Ein Himma	AH (13)	751600	3621710	#######	7.1	72	37.7	1130	4.84	118	32	8.89	1.9	84.4	150	125	1.06	291	8.4	-6.16	-31.13
16/19	Ein Himma	AH (16)	751661	3621700	#######	7.03	85	40	499	4.06	110	30	9.5	2	94	161	129	1.32	244	6.7	-6.13	-28.98
Springs (Golan Heights, cover basalt, fresh)																						
18/920	Umm Abu ad Dananir		763884	3648639	#######	6.68	468	17.8	349		22.4	13.7	5.69	0.25	23.8	25.7	11.8		128	0.06	-6.11	-27.3
18/921	Ayit fall		757703	3649486	#######	7.61	433	18	1010		85	43	4.47	0.83	64.5	108	24.9		408	0.02	-4.94	-21.6
18/922	Amphy spring		748804	3653081	#######	7.69	460	18.6	363		26.1	15.4	4.31	0.21	25.5	17.3	5.7		168	0.05	-6.97	-30.0
Springs (Mt. Hermon, limestone, fresh)																						
08/786	Ein Dan		751017	3682076	#######	7.39	445	15.9	472	3.44	65.9	5.44	0.65	0.09	4.34	9.77	8.99		211	1.01	-7.36	-38.34
08/787	Ein Banyas		746939	3682079	#######	7.49	497	18.4	358	3.52	72.3	12.4	1.46	0.30	9.87	12.9	57.3		206	1.00	-7.29	-37.59
	Average										69.1	8.92	1.06		7.11	11.3	33.1					
River																						
16/18	Yarmouk River	YR	756255	3624301	#######	8.4	191	23.5	961	3.18	55	30	5.7	0.57	97	110	147	0.2	184	5.9	-4.32	-21.34

Table 2: REY composition of the discussed groundwater from the Lower Yarmouk Gorge.

ID	Location	Short	La pmol/l	Ce pmol/l	Pr pmol/l	Nd pmol/l	Pm	Sm pmol/l	Eu pmol/l	Gd pmol/l	Tb pmol/l	Dy pmol/l	Y pmol/l	Ho pmol/l	Er pmol/l	Tm	Yb pmol/l	Lu pmol/l
01-128	Mukheibeh 1 2001	M1 (01)	2.35	4.31	0.58	2.33		0.48	0.17	0.54	0.09	0.70	17.71	0.17	0.72		1.01	0.20
13/803	Mukheibeh 2 2013	M2 (13)	1.40	2.11	0.28	1.14		0.22	0.08	0.35	0.06	0.54	14.84	0.14	0.58		0.86	0.17
16-08	Mukheibeh 2 2016	M2 (16)	2.21	3.75	0.43	1.98		0.74	0.08	0.42	0.06	0.65	18.59	0.17	0.67		0.89	0.17
13/802	Mukheibeh 4 2013	M4 (13)	1.51	2.47	0.31	1.42		0.26	0.08	0.29	0.06	0.44	11.57	0.11	0.48		0.72	0.13
16-09	Mukheibeh 4 2016	M4 (16)	22.21	41.72	5.15	21.76		4.34	1.02	3.99	0.54	3.43	52.06	0.70	2.10		1.89	0.31
16-12	Mukheibeh 5 2016	M5 (16)	1.18	1.84	0.18	0.81		0.23		0.09		0.11	2.90				0.16	
16-10	Mukheibeh 6 2016	M6 (16)	1.54	2.57	0.23	1.03		0.28		0.21	0.05	0.42	14.17	0.12	0.49		0.77	0.15
16-14	Mukheibeh 7 2016	M7 (16)	4.62	9.02	0.90	3.47		0.63	0.17	0.69	0.10	0.79	17.05	0.18	0.66		0.79	0.13
13/804	Mukheibeh 8 2013	M8 (13)	5.14	8.87	1.10	4.53		0.89	0.23	0.91	0.15	0.90	12.69	0.19	0.56		0.46	0.08
16-16	Mukheibeh 8 2016	M8 (16)	4.66	6.57	0.79	3.02		0.49	0.12	0.53	0.06	0.54	9.73	0.11	0.36		0.34	0.05
16-17	Mukheibeh 9 2016	M9 (16)	14.58	29.29	2.84	8.76		0.51	0.11	0.92	0.07	0.47	8.02	0.09	0.32		0.49	0.12
16-11	Mukheibeh 10 2016	M10 (16)	3.63	7.27	0.79	3.40		0.81	0.18	0.71	0.09	0.62	8.73	0.12	0.38		0.42	0.08
16-13	Mukheibeh 11 2016	M11 (16)	4.22	7.74	0.84	3.60		0.82	0.21	0.89	0.14	1.22	27.90	0.29	0.96		0.99	0.16
13/805	Mukheibeh 13 2013	M13 (13)	7.48	11.31	1.19	4.65		0.77	0.23	0.86	0.10	0.75	11.11	0.16	0.50		0.54	0.09
16-15	Mukheibeh 13 2016	M13 (16)	2.97	6.20	0.62	2.67		0.62	0.16	0.59	0.09	0.69	12.51	0.16	0.49		0.50	0.08
16-07	Meizar 1	Me1	1.40	2.21	0.18	0.96		0.42	0.28	0.53		0.18	3.23				0.14	
01-166	Meizar 2 2001	Me2 (01)	4.38	10.32	1.33	4.80		1.03	0.23	1.05	0.14	0.88	15.75	0.17	0.49		0.40	0.06
08/753	Meizar 2 2008	Me2 (08)	7.17	18.48	3.23	15.86		5.48	1.40	6.32	0.84	4.18	34.51	0.75	1.91		1.21	0.15
16-02	Meizar 2 2016	Me2 (16)	6.14	10.28	1.14	4.51		0.85	0.22	1.09	0.16	1.15	24.60	0.25	0.72		0.51	0.07
01-167	Meizar 3 2001	Me3 (01)	9.98	18.14	2.48	10.12		2.24	0.56	2.25	0.31	1.81	23.87	0.35	1.02		0.86	0.14
08/752	Meizar 3 2008	Me3 (08)	30.39	86.80	17.80	96.20		31.56	7.83	36.36	4.79	23.55	140.96	3.97	8.98		5.48	0.77
16-01	Meizar 3 2016	Me3 (16)	1.33	2.39	0.25	1.03		0.20		0.20	0.04	0.22	4.63	0.05	0.17		0.25	0.05
16-03	Ein Sahina	ES	1.84	3.24	0.32	1.43		0.28		0.33		0.35	9.18	0.09	0.30		0.30	0.04
16-04	Ein Balsam 2016	EB	4.68	9.13	0.98	4.20		0.75	0.20	0.80	0.10	0.76	17.16	0.16	0.53		0.61	0.10
00- 108	Ein Makla 2000	ER (00)	12.49	25.59	1.87	11.20		1.81	0.49	2.16	0.33	2.26	50.15	0.55	1.91		2.03	0.35
04-586	Ein Makla 2004	ER (04)	10.31	14.67	1.81	7.43		1.28	0.38	1.83	0.31	1.99	47.02	0.48	1.84		1.92	0.33
16-06	Ein Makla 2016	ER (16)	8.81	11.05	1.44	6.23		1.26	0.38	1.70	0.27	2.23	50.26	0.52	1.84		2.03	0.36
00- 107	Ein Reach 2000	EM (00)		19.71	1.46	9.53		1.35	0.38	1.50	0.24	1.50	27.60	0.31	1.17		1.25	0.22
04-585	Ein Reach 2004	EM (04)	4.75	7.70	0.98	3.61		0.62	0.21	0.84	0.15	1.04	19.69	0.22	0.73		0.92	0.17
16-05	Ein Reach 2016	EM (16)	14.61	25.69	2.88	12.01		2.16	0.60	2.41	0.33	2.40	43.53	0.53	1.75		1.72	0.30
16-20	Ain Saraya	AS	12.27	18.80	2.33	7.34		0.49	0.11	0.84	0.08	0.64	15.98	0.16	0.62		0.85	0.17
01-12	Ain Himma 2001	AH (01)	4.31	23.39	3.48	13.06		2.98	0.78	3.38	0.52	3.33	51.76	0.73	2.21		2.02	0.34
07/624	Ain Himma 2007	AH (07)	16.34	65.43	3.42	14.15		3.38	0.92	4.19	0.68	4.29	62.85	0.93	2.79		2.57	0.42
13/807	Ain Himma 2013	AH (13)	4.06	7.58	0.74	2.91		0.53	0.13	0.53	0.09	0.61	13.83	0.16	0.52		0.66	0.11
16-19	Ain Himma 2016	AH (16)	43.50	61.06	8.54	25.95		0.76	0.19	2.11	0.12	0.92	19.85	0.21	0.80		1.05	0.23

Table 2: Continued.

ID	Location	Short	La pmol/l	Ce pmol/l	Pr pmol/l	Nd pmol/l	Pm	Sm pmol/l	Eu pmol/l	Gd pmol/l	Tb pmol/l	Dy pmol/l	Y pmol/l	Ho pmol/l	Er pmol/l	Tm	Yb pmol/l	Lu pmol/l
08/787	Ein Banyas	EBY	45.10	5.39	9.80	45.24		8.29	2.26	10.58	1.52	11.14	249.79	2.71	8.08		6.35	0.96
08/786	Ein Dan	ED	50.63	23.07	12.00	54.53		10.48	2.86	12.74	1.82	12.55	240.58	2.91	8.78		7.57	1.22
16-18	Yarmouk	YR	38.37	82.25	8.18	34.96		5.88	1.53	6.64	0.83	5.92	153.95	1.43	4.93		5.54	1.07

TABLE 3: Sr^{2+} concentration and $^{87}Sr/^{86}Sr$ isotope signatures of groundwater and rocks from the Lower Yarmouk Gorge and surrounding areas.

ID	Well/spring	Sr (mg/l)	$^{87}Sr/^{86}Sr$
16/08	Mukheibeh 2	0.51	0.70769
16/09	Mukheibeh 4	0.5	0.70764
16/12	Mukheibeh 5	0.94	0.70770
16/10	Mukheibeh 6	0.66	0.70767
16/14	Mukheibeh 7	0.54	0.70757
16/16	Mukheibeh 8	1.3	0.70748
16/17	Mukheibeh 9	5.3	0.70778
16/11	Mukheibeh 10	0.96	0.70757
16/13	Mukheibeh 11	0.87	0.70767
16/15	Mukheibeh 13	0.88	0.70757
16/07	Meizar 1	2.1	0.70754
16/02	Meizar 2	5.5	0.70760
16/01	Meizar 3	1.1	0.70755
16/03	Ein Sahina	0.56	0.70763
16/04	Ein Balsam	3.5	0.70765
16/06	Ein Makla	5.5	0.70767
16/05	Ein Reach	4.2	0.70776
16/20	Ain Saraya	3.8	0.70771
16/19	Ain Himma	2	0.70759
18/920	Umm Abu ad Dananir	0.252	0.70458
18/922	Amphy spring	0.21	0.70457
16/18	Yarmouk	0.57	0.70708
ID	Rock sample	Sr (mg/kg)	$^{87}Sr/^{86}Sr$
18/A	Golan Heights 1	1934	0.70330
18/B	Golan Heights 2	1040	0.70350

varied over the years. Hamat Gader brines are lower in SO_4^{2-} but higher in Cl^- and Br^- than Meizar brines. Waters from wells such as Meizar 1 and Mukheibeh 8, 9, and 11 sometimes deviate from the indicated trend lines. The Yarmouk River water is mostly comparable to Mukheibeh water, but not in diagramms with Na^+, Cl^- and SO_4^{2-}.

4.2. Uranium. U(VI) is correlated neither with any other element mentioned before nor with Eh varying between -200 and +200 mV (Table 1). The Mukheibeh field splits into three subgroups (Figure 5). U(VI) with 80-105 nmol/l has the highest values in Mukheibeh groundwater. Groundwater from wells Mukheibeh 5 and 11, Ain Himma, Hamat Gader shows values between 3 and 10 nmol/l. The groundwater with <0.1 nmol/l and that with U(VI) below the detection limit comprise all well waters from Meizar 2 and 3 and Mukheibeh 1, 8, and 9. The lowest U(VI) values are either in the lowest or in the highest sulfate groundwater (Figure 5(b)).

4.3. Rare Earths and Yttrium. Weathering of omnipresent alkali olivine basalts in the Yarmouk basin releases Fe(II) which precipitates as colloidal ferric oxyhydroxides (HFO) under oxidizing conditions. These colloids later aggregate to gels on all solid surfaces along the pathways within and below the basaltic layer. In aqueous systems, however, HREE and Y are slightly fractionated. The REY patterns of samples in this study are subdivided into 6 types. The first group (t1) typifies groundwater derived from weathered alkali olivine basalts. The patterns t2 and t3 show the results of increasing mixing with limestone water (t4) (Figures 6(a)–6(d)). In Figure 6(e), three REY patterns of type t2* are compiled which show very high LREE contents but low HREE and Y. Otherwise, they resemble type t2. Another different feature of t2* is that positive Gd anomalies exceed those of Y.

All of the above patterns show positive Y anomalies. The dissolution of REY-enriched HFO yields convex patterns of type t5 with enhanced abundances of medium REE compared to light and heavy REE and negative Y anomalies (Figure 6(f)). These Y anomalies develop because Y prefers to stay in the aqueous phase during the stage of REY adsorption by HFO [36].

The water from Ain Himma in 2001 and 2007 and well Mukheibeh 4(16) shows REY patterns, typical of water from limestone aquifers such as those of Ein Dan and Ein Banyas in the Mt. Hermon Massif but without the negative Ce anomalies typical of spring waters from karstic limestones (Figure 6(g)) or from Cretaceous limestones along the rift valley [37]. Note that the REY abundance in waters from Mukheibeh 4(16) and Ain Himma from years 2000 and 2007 is lower than that in the spring waters of Dan and Banyas, which may be a result of interaction with HFO.

4.4. $^{87}Sr/^{86}Sr$. Although the waters show a wide spread in Sr^{2+}, their $^{87}Sr/^{86}Sr$ isotope ratios vary only between 0.7070 and 0.7077 (Figure 7). This corresponds with the range of $^{87}Sr/^{86}Sr$ in Cretaceous limestones of Israel, which is about 0.7070-07086 (Wilske et al., unpublished data). Only the Yarmouk River with 0.70710 points to mixing with basaltic rock drainage water which shows an $^{87}Sr/^{86}Sr$ value of 0.70455, slightly above Phanerozoic upper mantel alkali olivine basalts from Israel with $^{87}Sr/^{86}Sr$ of 0.7033-07035 (Table 3).

In the plot of Sr^{2+} vs. $^{87}Sr/^{86}Sr$, Mukheibeh field groundwater clusters at low Sr^{2+}, whereas the samples from Hamat Gader, Meizar 2, and Himma show a wide spread. Mukheibeh 8 water fits into the Hamat Gader-Meizar 2-Himma trend, whereas Meizar 3 approaches the Mukheibeh field.

4.5. $\delta^{18}O$ vs. δD. The stable water isotopes in the LYG range from low values of Meizar 2 in the southern Golan Heights and springs and wells on the eastern plunge of the Mt. Hermon Massif towards the Hauran plateau to high values in water of the Yarmouk River (Figure 8). All data from the LYG are plotted between the Syrian and Mt. Hermon meteoric water lines (MWL). The Mukheibeh waters like the groundwater from the Hauran plateau nearly cover the whole array, whereas the samples of Meizar, Hamat Gader, and Himma cluster. Ein Sahina, located uphill of the Hamat Gader group, is plotted among the Mukheibeh field. Ain Sarayah, located close to Ein Reach of the Hamat Gader

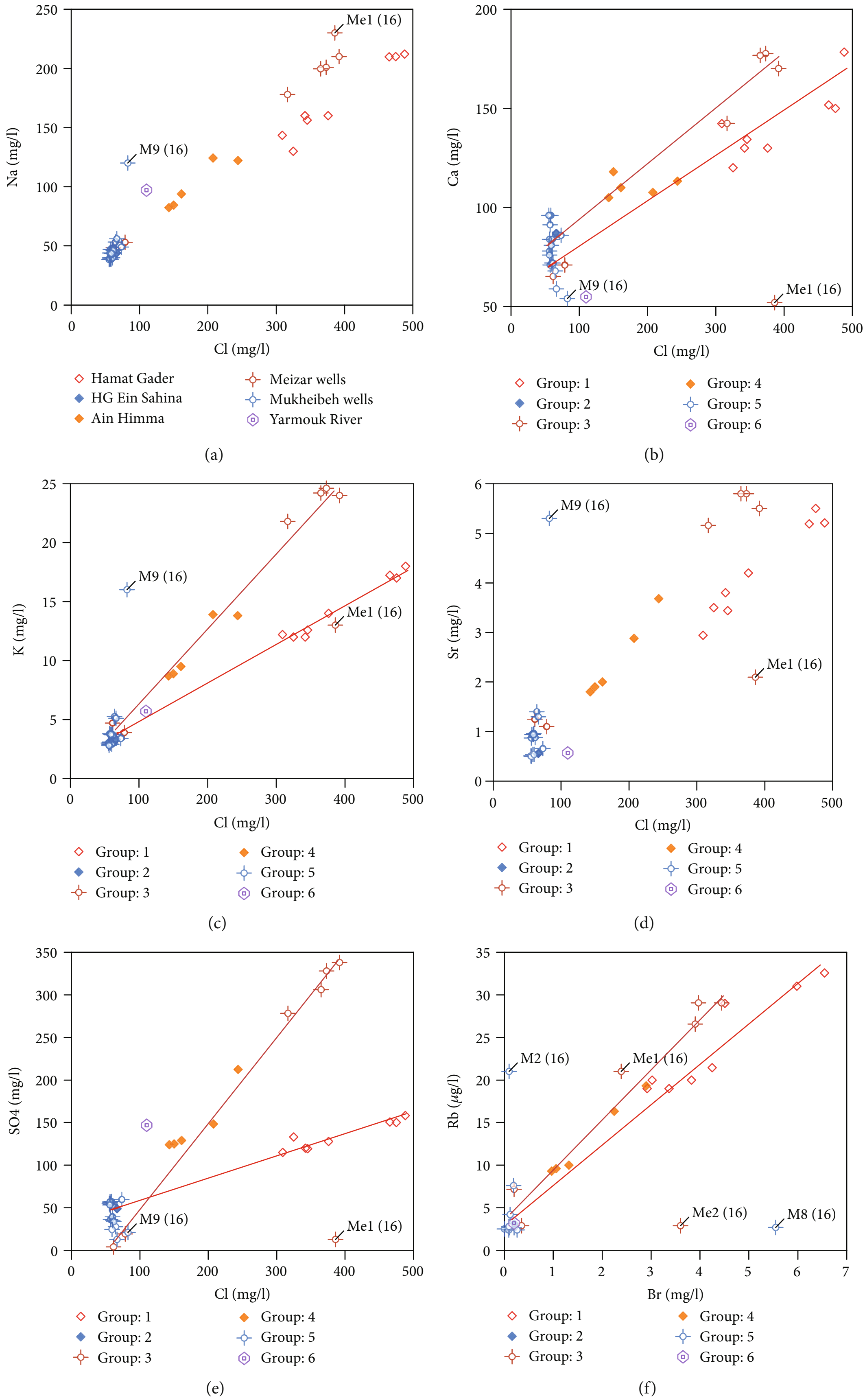

Figure 4: Continued.

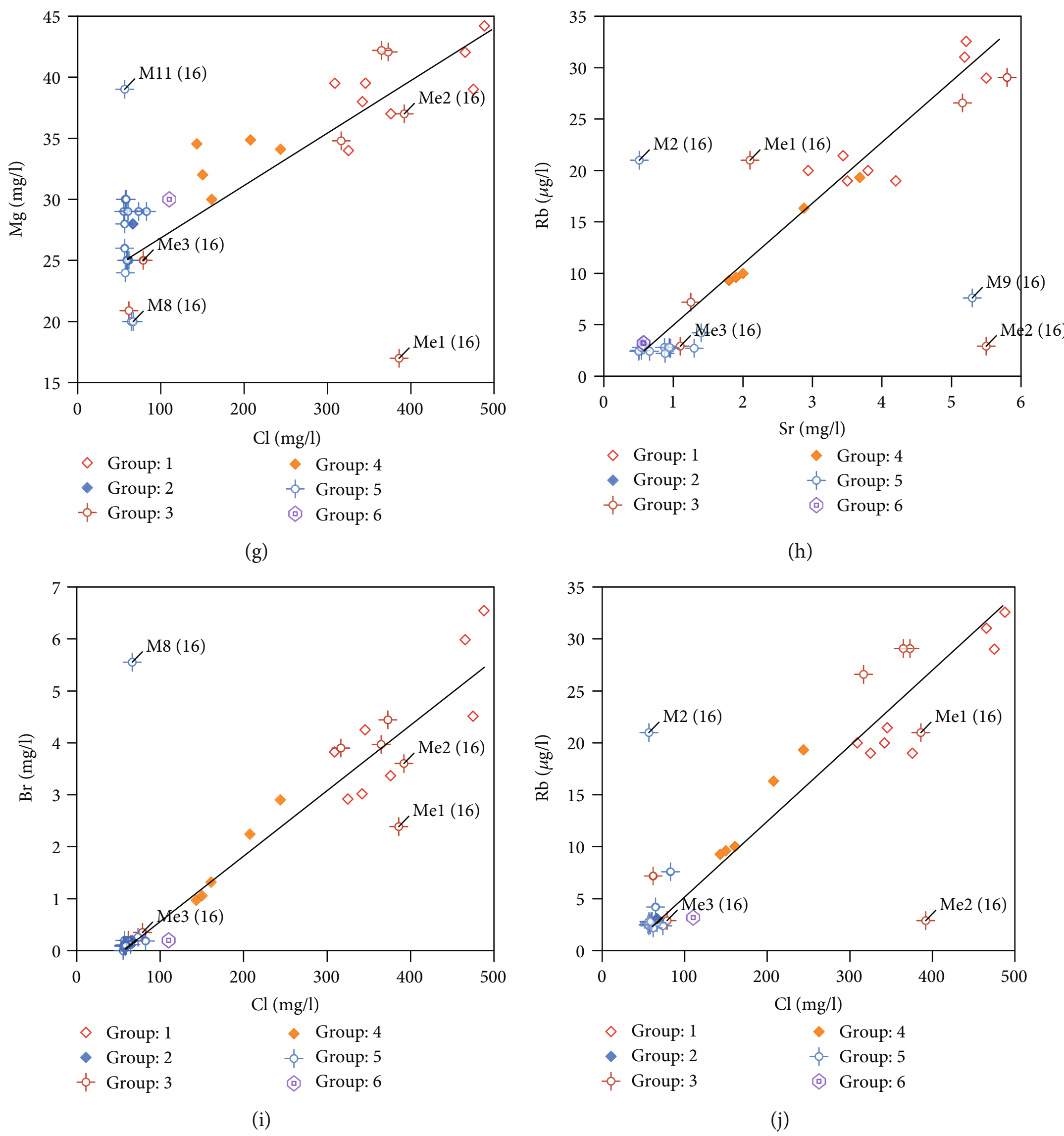

FIGURE 4: Crossplots of elements in the groundwater in the Lower Yarmouk Gorge. For details, refer to text.

cluster, is plotted among the heaviest Mukheibeh waters. Meizar 2 and Meizar 3(08) show the lowest isotope values.

5. Discussion

5.1. Sources of Groundwater. The stable isotopes of water and the element correlations reveal different origins of fresh and saline contributions to the groundwater in the LYG. Distinct groups of stable isotopes suggest regional infiltration areas at different elevations. The Meizar 2 groundwater from 2001 to 2016 with (i) light δ^2H and δ^{18}O signatures and (ii) REY patterns of nearly limestone water shape and least affected by HFO (t4 in Figure 6(d)) suggests infiltration of precipitation on the outcropping Triassic to Cretaceous limestones of the foothills of the Mt. Hermon Massif. The increase in Cl^- is higher than that in Na^+ probably pointing to mobilization of highly evaporated seawater brines and admix of these brines to the limestone water.

The water of Meizar 2(08) and Meizar 3(08) shows similar chemical and isotopic composition and the same type of REY patterns (t5). Although showing similar U(VI) concentrations, Meizar 2(01) and Meizar 2(16) are dissimilar in REY patterns (t4 and t5). This suggests that these types of groundwater discharge from the same reservoir but the flow path of recharging water differs over the years.

The groundwater with δ^{18}O and δD of about -6‰ and -30‰, respectively, typifies the groundwater from Hamat Gader, Himma, Meizar 3 in 2001 and 2016, and the Mukheibeh field. Most of the Mukheibeh and Hauran groundwater shows a trend of increasingly heavy stable isotopes of water, suggesting evaporation of recharge prior to infiltration (Figure 8). The effect of evaporation on stable isotope enrichment is shown by heaviest δD and δ^{18}O signatures in the Yarmouk River.

High molar values of Na^+/Cl^- and Ca^{2+}/SO_4^{2-} but low Br^-/Cl^- and low concentrations of Na^+, Cl^-, Ca^{2+}, Mg^{2+}, K^+, Sr^{2+}, and Br^- typify the basaltic waters [31]. Pure basaltic

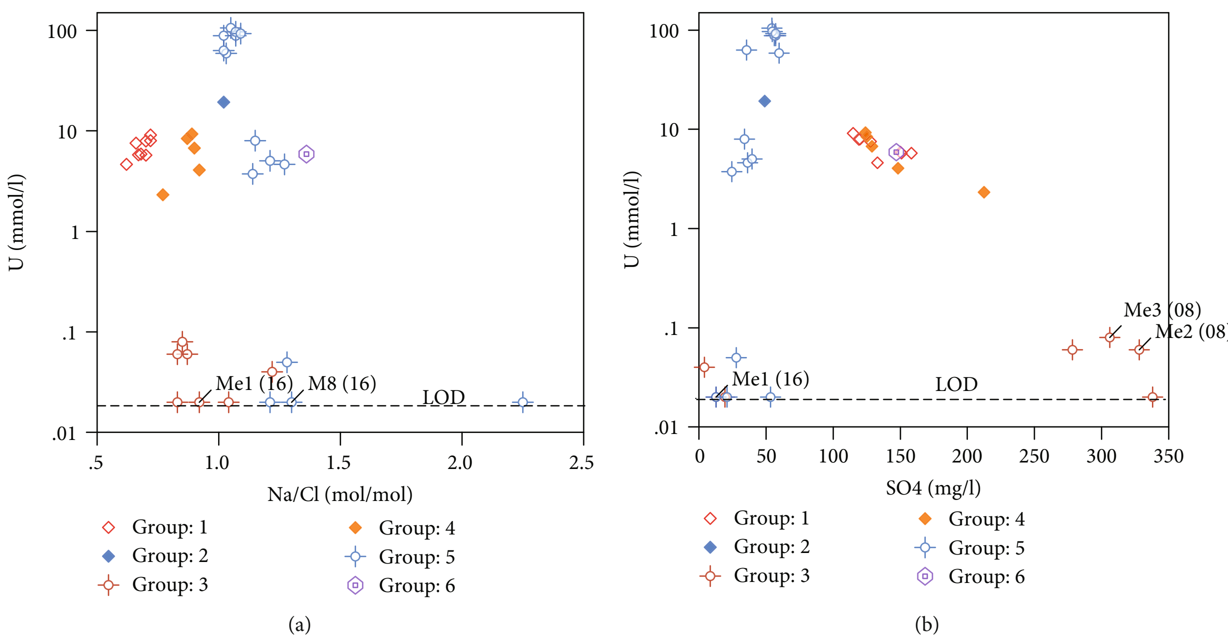

Figure 5: Crossplots of U(VI) and Na/Cl values in the groundwater of the Lower Yarmouk Gorge.

water is characterized by $Na^+/Cl^- \gg 1$ (Table 1) and typical REY patterns of type t1 (Figure 6(a)). With increasing leaching of halite from sedimentary rocks, the basaltic waters approach the lowest Na^+/Cl^- value of about 1, whereas mixing with evaporated seawater brines yields $Na^+/Cl^- < 1$ (Figure 9). Comparison of the Mukheibeh waters with those of basaltic composition reveals that the former waters are enriched in all elements (Table 1). The dissolution of anhydrite/gypsum by thermal waters of Meizar and Himma leads to enhanced concentrations of Ca^{2+} and SO_4^{2-} (Figure 4(b)). Ca^{2+} may also increase by dissolution of calcite at enhanced temperatures and albitization of plagioclases in basalts. Mg^{2+}, Rb^+, Br^-, and K^+ may be gained by ion exchange against Ca^{2+} in marly layers in the aquifers (Figures 3 and 4). A Br^- increase may be gained by contact with the bituminous-rich B2 formation. The correlations of Cl^- with SO_4^{2-}, Ca^{2+}, Mg^{2+}, Sr^{2+}, Rb^+, and Br^- reveal that, with few exceptions, waters from Hamat Gader, Himma, and Meizar are mixtures of basaltic water and remnants of brines from the Triassic-Cretaceous Arabian carbonate platform. The strong correlation of Rb^+ and Sr^{2+} indicates a common source but not necessarily the same mineral (Figure 4(h)). The two trends in the correlation of Rb^+ and Br^- verify the different sources of both elements (Figure 4(j)).

The molar $1000Br^-/Cl^-$ vs. Na^+/Cl^- values show several trends for groundwater in the Yarmouk basin and the trend of evaporated seawater in salt pans (Figure 9). In this plot, the springs of Hamat Gader, Himma, and well Meizar 2 define vertical trends which are only explainable by leaching of Br^- from the organic-rich B2 formation (Figure 3). Meizar 3 in 2001 and 2016 and all the groundwater with the lowest Br^-/Cl^- values in the vertical groups suggest mixing between Mukheibeh groundwater and seawater brine characterized by Na^+/Cl^- and $1000Br^-/Cl^-$ of about 0.5 and 5.3, respectively. Such ratios resemble those of the Ha'On type of brine, emerging at SE shoreline of the Lake Tiberias [2, 38, 39]. A second mixing line is indicated by Ein Sahina and Mukheibeh wells 1 and 6; both lines only differ in the Mukheibeh end member.

5.2. The Impact of HFO Precipitation on U and REY. U(VI) is highly adsorbed onto the high surface area of HFO [40]. The U content of alkali olivine basalts is in the range of 1 ppb [41]. The infiltrating basaltic groundwater with low U(VI) content passes the growing HFO "filter" within and below the basaltic cover of the Hauran plateau and elsewhere. During the alteration of HFO to goethite, lepidocrocite, or hematite, the adsorbed U(VI) is reduced to U(V) which is more resilient to oxidation than uraninite (UO_2) or adsorbed U(IV) [42, 43]. Adsorption of U(VI) in the pH range of 6.6-7.3 (Table 1) is not affected by additional adsorption of phosphate [44].

The high U(VI) contents of 80 to 105 nmol/l in the groundwater of Mukheibeh artesian wells 1, 2, 4, 6, and 7 are most probably supplied later from the phosphorite-rich B2 aquifer. The phosphorites from the B2 formation in Syria, Jordan, and Israel contain about 100 ppm U [45]. Assuming that U(VI) is mobilized by phosphate as $UO_2(HPO_4)_2^{2+}$ [46], the phosphate concentration should be in the range of 0.2 μmol/l or 6 μg/l which was much below our routine detection limit of phosphate of 1 mg/l.

Meizar 2 water has its source in the flanks of the Mt. Hermon Massif and in the western elevations of the Hauran plateau, which agrees with light stable isotopes of water. Although limestone waters contain 2-20 nmol/l U(IV) from elsewhere in Israel (Siebert unpublished), Meizar 2 and Mukheibeh 8, 9, and 11 waters show less than 0.1 nmol/l U(VI) suggesting that these waters must have had contact with HFO but did not interact with the B2 formation. Though having similar low U, considerably heavier stable isotope signatures in Mukheibeh 8 and 9, the most

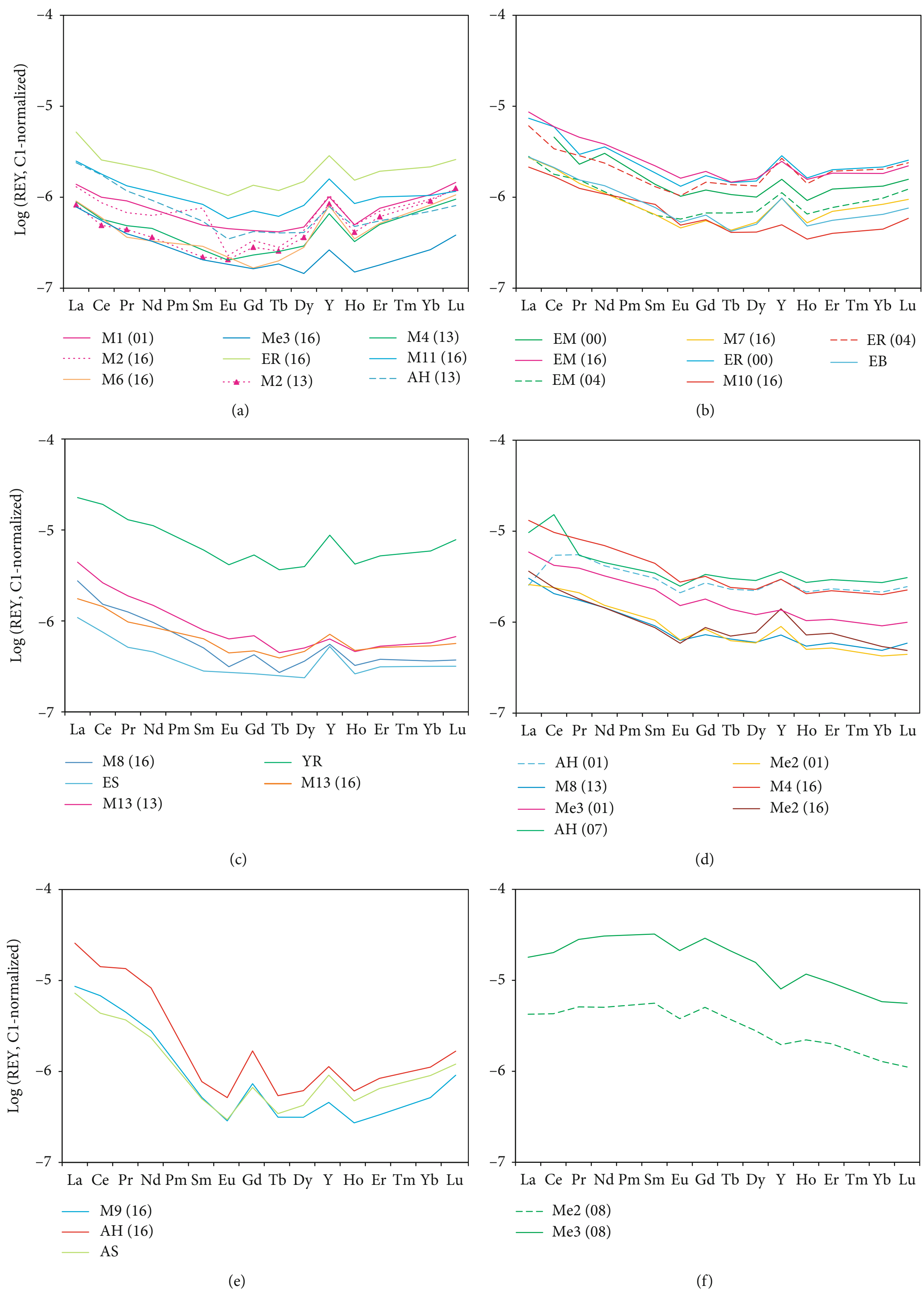

Figure 6: Continued.

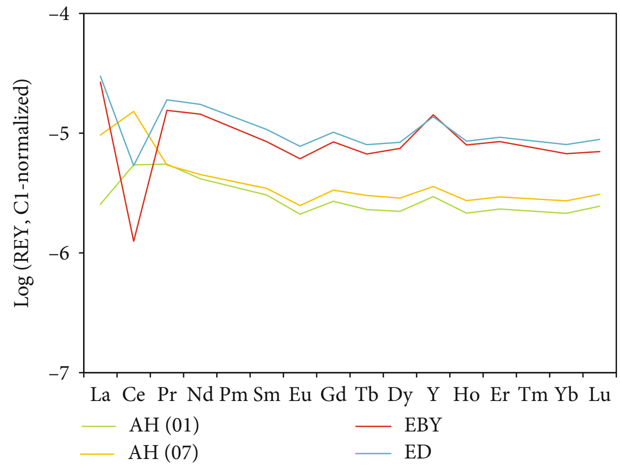

(g)

FIGURE 6: REY distribution patterns of groundwater in the Lower Yarmouk Gorge. The visual grouping of patterns shows their high variability.

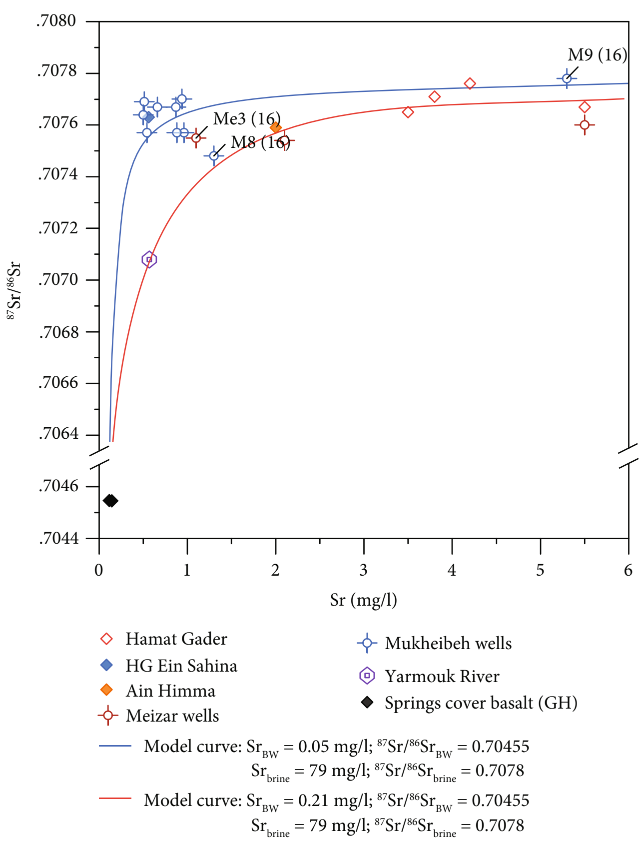

(a)

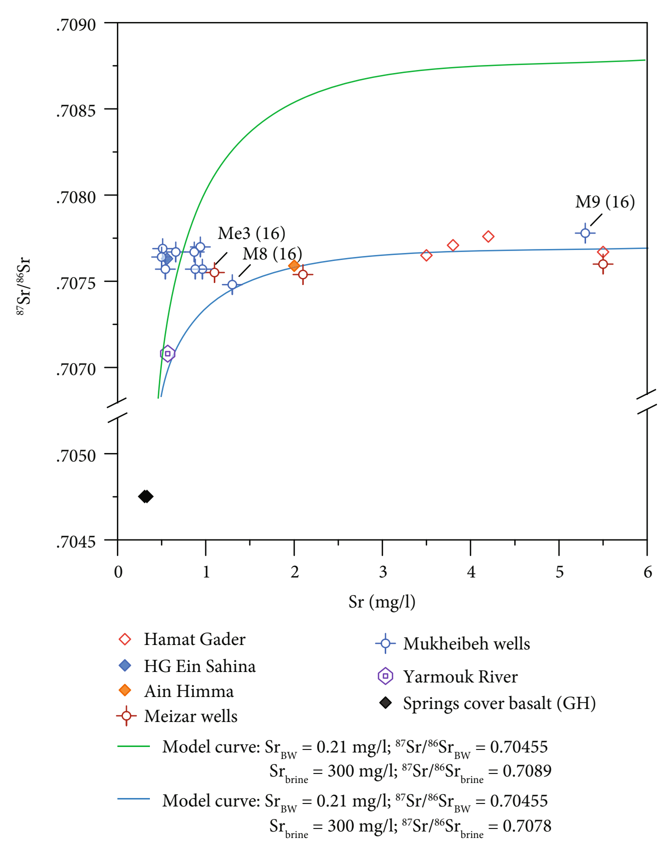

(b)

FIGURE 7: Crossplots of Sr isotope ratios and Sr^{2+} in the groundwater from the Lower Yarmouk Gorge.

northeastern samples in the LYG, refer to a recharge area differing from Meizar 2.

HFO scavenges not only U(IV) but also REY and HPO_4^{2-}. There may be some synergetic interaction between phosphate and REY resulting in type t1 patterns. This seems to be indicated in type t2*, which is possibly due to Y-phosphate precipitation (possibly churchite, Y, and $HREEPO_4$) due to which the light REE are released [47].

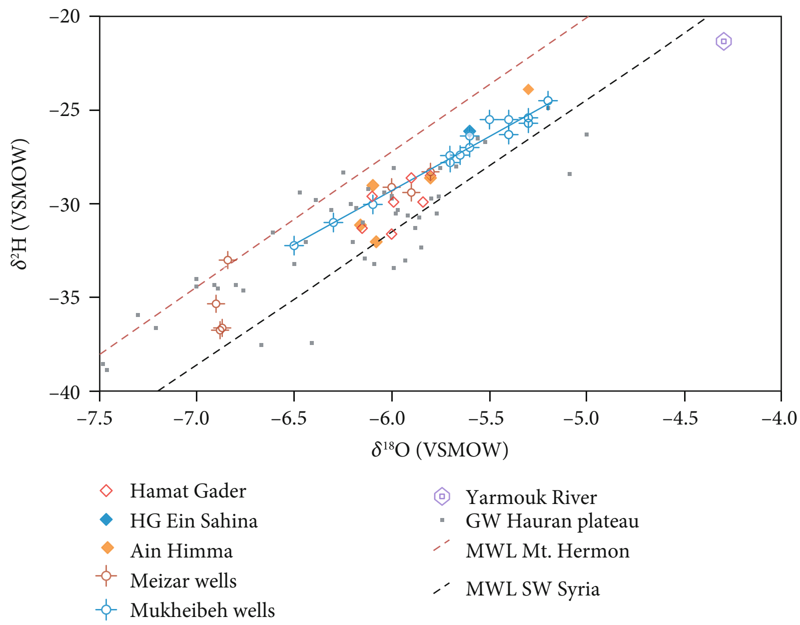

Figure 8: δD vs. $\delta^{18}O$ in groundwater of the Lower Yarmouk Gorge ([1]; this study) and the Hauran plateau [18]. MWL for Mt. Hermon and SW Syria are taken from Brielmann [52] and Al Charideh and Zakhem [53], respectively.

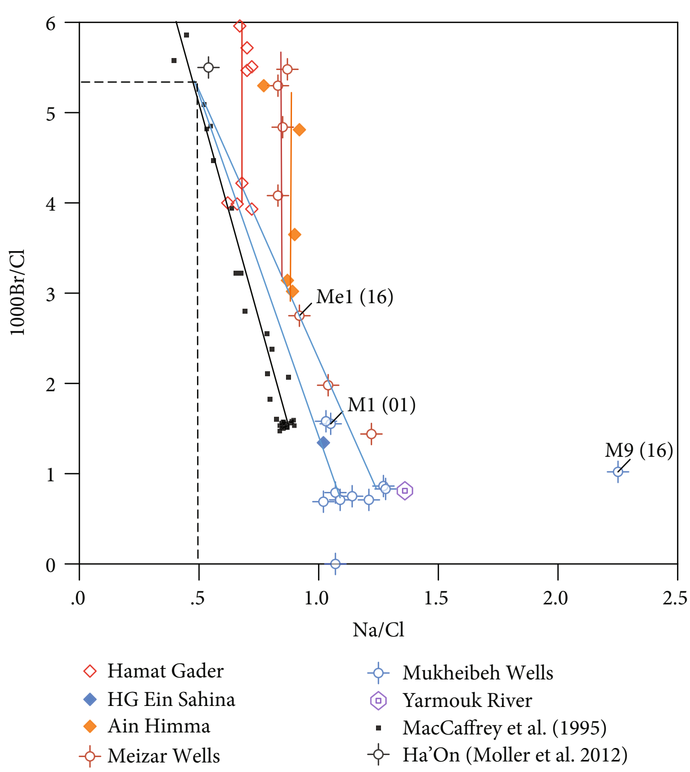

Figure 9: Crossplots of 1000Br/Cl and Na/Cl of the groundwater from the Lower Yarmouk Gorge.

All groundwater in the gorge is produced from limestone aquifers. When the REY poor basaltic water passes the limestones at enhanced temperatures, some calcite dissolves and thereby its aliquot of REY is released and mixed with REY load of the groundwater. More than 99% of the REY is immediately adsorbed onto calcite surfaces [48]. This way, the REY patterns of groundwater change from type t1 to t2, t3, and finally t4 (Figures 6 and 10). At enhanced

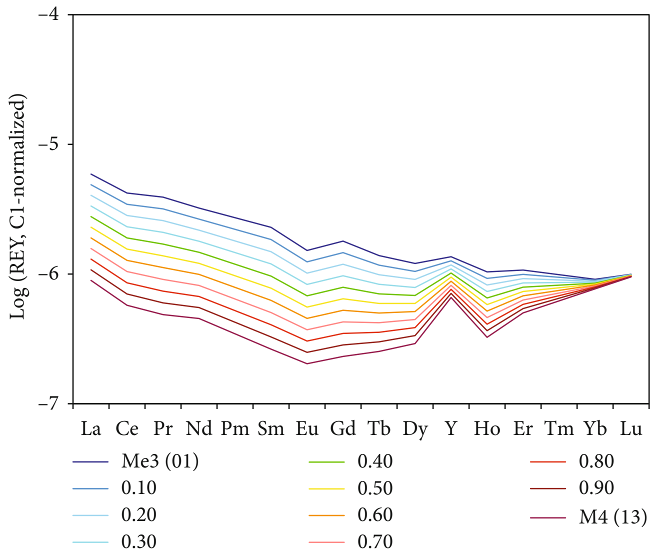

FIGURE 10: Mixing of basaltic and limestone groundwater showing the change in rare earth distribution patterns.

temperatures, release of LREE is faster than that of HREE and Y because their Coulomb binding forces are less for the former bigger than the latter smaller ions. This may qualitatively explain the change in REY patterns of groundwater in the Yarmouk basin.

Although the groundwater of the Yarmouk Gorge is produced from limestone aquifers, their REY patterns still indicate that the groundwater originates from basaltic catchment regions or, more precisely, has passed HFO layers. Although the patterns are similar in shape, the spring waters of Dan and Banyas from limestones of the Mt. Hermon Massif without contact with HFO show higher abundances than the limestone-like waters from the Yarmouk Gorge such as in Himma spring and Mukheibeh well 4(16) (Figure 6(g)). Types t1 to t4 in Figure 5 represent the continuous change of REY patterns due to the interaction of basaltic groundwater after passing the HFO filter t1 and limestones resulting in changes according to t2-t4. These types of patterns result from mixing limestone and basaltic rock waters. It could well be that not the whole volume of water changes due to the interaction but only parts of it and mixing of various types yields the final patterns as shown in Figure 10.

Type t5 (Figure 6(e)) is not showing dissolution of phosphate minerals such as apatite but leachates of altering HFO that loses REY at high levels. The difference between the latter two is that the former should show a positive Eu anomaly [36], whereas the latter is characterized by a negative one.

How does it come that these types of groundwater still show REY patterns typical after infiltration in basaltic catchment areas? The reason is that the REY in calcite surfaces along the pathways in limestones equilibrate with the low REY abundance from the basaltic catchment. Under steady-state conditions, the groundwater from limestones shows patterns achieved by the interaction with groundwater that has passed HFO layers [31].

5.3. *Tracing Mixing by Sr^{2+} and $^{87}Sr/^{86}Sr$.*

The above discussed findings, which trace back the genesis of the groundwater in the LYG by variable interactions of basaltic water with late Tertiary brines of Ha'On type and with calcite and limestone of the discharging Cretaceous/Paleogene aquifers, can be fortified by model calculations, which try to resemble the measured $^{87}Sr/^{86}Sr$ values in the groundwater of the LYG by at least interaction of basaltic water and brine (Figure 7).

Using the fraction ε_{brine} of brine in the mixture of brine and basaltic water, the mix of Sr^{2+} (Equation (1)) and the mix of the Sr^{2+} isotope ratios (Equation (2)) are estimated.

$$Sr_{mix} = \varepsilon_{brine} \times Sr_{brine} + (1 - \varepsilon_{brine}) \times Sr_{BW}, \tag{1}$$

$$\begin{aligned} {}^{87}Sr/{}^{86}Sr_{mix} = {}& {}^{87}Sr/{}^{86}Sr_{brine} \times \varepsilon_{brine} \times Sr_{brine}/Sr_{mix} \\ & + {}^{87}Sr/{}^{86}Sr_{BW} \times (1 - \varepsilon_{brine}) \times Sr_{BW}/Sr_{mix}, \end{aligned} \tag{2}$$

where index BW is the basaltic water.

Considering the analytical data on Sr^{2+} concentration of groundwater in Table 3, brine, basaltic water, and dissolved calcite and gypsum and their corresponding $^{87}Sr/^{86}Sr$ values and the Sr^{2+} concentration of basaltic water must be below 0.5 mg/l, the lowest value in Mukheibeh water. Indeed, pure basaltic water sampled from 2 springs in the cover basalt of the Golan Heights shows $Sr^{2+} = 0.2$ mg/l. The Sr^{2+} concentration of the brine may be between 79 mg/l as analyzed in Ha'On brine [2] and 300 mg/l, depending on the amount of dissolution of calcite from limestone with assumed average Sr^{2+} concentrations of 100 mg/mol calcite and about 25 mg/mol gypsum from evaporites [49]. The $^{87}Sr/^{86}Sr$ value of basaltic water is 0.70455 to 0.70457, and that of the brine is assumed to be 0.7078, matching the spread of data in Figure 7. The $^{87}Sr/^{86}Sr$ value of 0.7078 may result from mixing of Late Tertiary Tethys

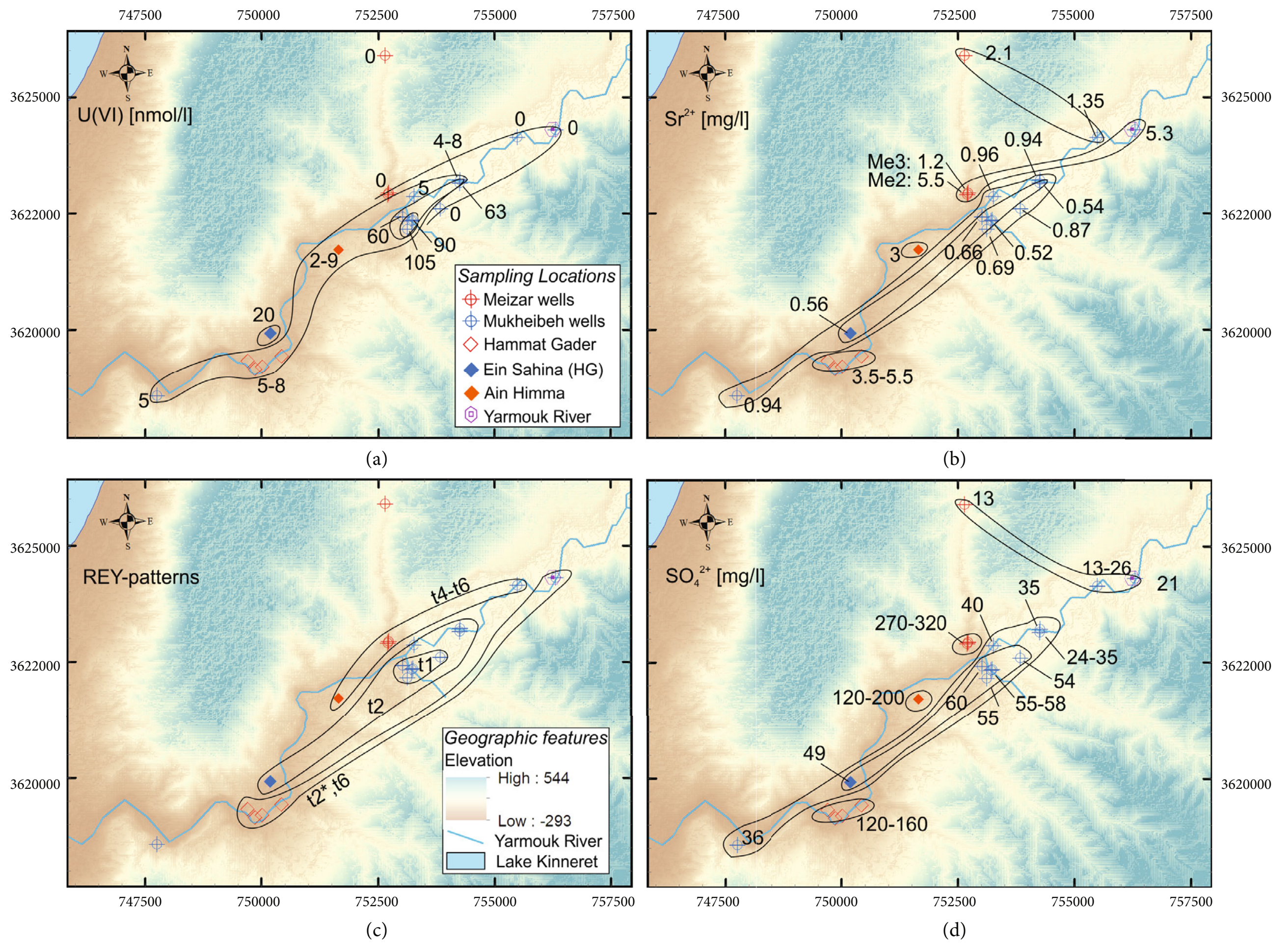

FIGURE 11: Regional distribution of U(VI) (a), Sr^{2+} (b), rare earth distribution patterns (c), and sulfate (d) in the Lower Yarmouk Gorge. Legends given in (a) and (c) are representative for the entire Figure 11.

seawater of 0.7089 [50] and dissolved average Upper Cretaceous limestone in Israel ranging between 0.7076 and 0.7078 (Wilske et al., unpublished data).

The model curves in Figure 6 are fitted by varying Sr^{2+} in basaltic water and in brine as well as the $^{87}Sr/^{86}Sr$ value of the brine. Several information can be derived by the following procedure.

(1) The observed groundwater cannot be fitted by one curve, and the results are sensitive to assumed values of $^{87}Sr/^{86}Sr$ and the resulting ε_{brine}

(2) To fit most Mukheibeh groundwater and that of Me3(16), the requested Sr^{2+} concentrations must be 0.05 mg/l, much lower than the observed 0.21 mg/l (Figure 7(a)). Hence, the positive shift of these types of groundwater along the ordinate is assumed to result from the interaction of the proposed fluid mix with calcite and gypsum in the discharging limestone aquifers, which show $^{87}Sr/^{86}Sr$ values as high as 0.7078 (Wilske et al., unpublished data)

(3) The fitting curves are invariant in respect to variations of Sr^{2+} in the brine (compare red curve in Figure 6(a) and blue curve in Figure 7(b))

(4) If $^{87}Sr/^{86}Sr$ values of brine are larger than 0.7078, neither the group of groundwater from Mukheibeh wells and Meizar 3 nor the group of Hamat Gader, Meizar 2, and Ain Himma can be represented (Figure 7(b))

In summary, the $^{87}Sr/^{86}Sr$ of the groundwater in the LYG is the result of relic brine, which is diluted by basaltic water and subsequently dissolves calcite and gypsum and experiences some exchange of Ca^{2+} against Mg^{2+}, Na^{+}, and K^{+} in marly layers of the aquifers (Figure 3). Only Meizar 3 is mainly limestone water.

5.4. Regional Distribution of Dissolved Species. The regional distribution of U(VI), Sr^{2+}, and REY shows comparable structures, whereas SO_4^{2-} behaves differently. High and low U(VI) concentrations are present in the NE of the Lower Yarmouk Gorge (Figure 11(a)). The high values of 80-105 nmol/l U mark the area in which Mukheibeh wells 1, 2, 4, 5, 6, and 7 produce artesian water from the phosphorite-rich B2 aquifer. These high U(VI) concentrations decrease to 20 nmol/l SW-ward, downstream the Yarmouk River and to both sides of the gorge. North of and NE-ward in the gorge groundwater contain U(VI) below 1 nmol/l. Such low values can only be established by adsorption of U(VI). In the case of

Mukheibeh 8 and 9, this could be HFO in the Hauran plateau; in the case of Meizar, saline groundwater contact with dissolving HFO is documented in Figure 7(f) in the year 2008. According to Shimron [51], basaltic intrusions are present in the Mt. Hermon anticline, being probably responsible for the low U(VI). Additionally, the long pathway through the limestone aquifers from Mt. Hermon to the LYG altered the REY patterns in groundwater to type t4. In 2016, Meizar 3 shows the REY pattern of type t1. However, in 2001, it resembled type t4 of Meizar 2 in 2001 and 2016.

In the central part of the LYG, Sr^{2+} is about 0.55 mg/l (Figure 11(b)), while it increases to 1 mg/l NE-ward, to 3 mg/l in Himma, to 4 mg/l in Hamat Gader, and to 5 mg/l in both Meizar wells 2 and 3.

A similar shell-like behavior is observable in the REY patterns with t1 patterns in the center followed by t2 SW-ward and t3 type SE-ward and patterns of t4 to t6 in the NW (Figure 11(c)).

The high-uranium water shows SO_4^{2-} concentrations of 30-50 mg/l (Figure 11(d)). Outside that central part, the groundwater shows either much higher SO_4^{2-} concentrations, such as in Hamat Gader (150 mg/l) and Meizar (300 mg/l), or almost no dissolved sulfate as in the NE (0.12 mg/l). The increasing SO_4^{2-} outside the marked center may prove depletion of gypsum in the central region of ascending groundwater. Comparing spatial concentration distribution patterns of Sr^{2+} and SO_4^{2-} results in similar patterns, though the concentration levels differ significantly.

Leaching of brines and/or evaporites alters the chemical composition of the initial basaltic water. The light signatures of water isotopes of Meizar 2 support a catchment area at the Mt. Hermon foothills or at elevated places in the Hauran. Meizar 3 water isotopes correspond with those of Hamat Gader and Himma, which may be taken as an indirect proof for its basaltic water. Their variable REY patterns of types t1, t4, and t5 suggest various flow paths of the groundwater including differing contacts with HFO. The shortest pathway of groundwater flow is indicated by REY patterns of type t1 (Figure 6), while patterns of type t2 and t3 suggest a longer pathway with more intense REY exchange with calcite in limestones. The longest pathways are typified by REY pattern type t4. The REY types and the concentrations of U(VI), Sr^{2+}, and SO_4^{2-} characterize complex flow patterns of groundwater towards the gorge.

The most distinct basaltic water is produced from the B1/B2 limestone aquifers fractured by a complex fault system crossing the LYG [15] (Figure 1(b)). This marks the most important flow path of drainage water from the Hauran into the LYG. The springs of Hamat Gader (including Ein Sahina) and Himma are positioned on an uptilted block, whereby both spring fields are separated from the Meizar field. The deep aquifer which is tapped by Meizar 2 also produced water in the shallow well Meizar 3 in 2008.

Although producing from the same aquifer, the hydrochemical differences in groundwater from Ein Himma and Meizar 3 disprove any transboundary flow below the Yarmouk River. The confined water from basaltic infiltration areas in Syria, however, is present on both sides of the gorge.

6. Conclusions

The conjoint study of major, minor, and trace elements, $\delta^{18}O$, δD, and $^{87}Sr/^{86}Sr$ in the groundwater of the LYG reveals the following:

(i) Mixtures of water from basaltic rocks and limestones are almost omnipresent in the LYG. A clear exception is Meizar 2 that produces groundwater that was infiltrated at the flanks of Mt. Hermon Massif. The mixtures vary from nearly pure basaltic water to nearly pure limestone water. In addition, leaching of residual brines and evaporites enhances the salinity of the various types of groundwater

(ii) The sources of salinization in limestone aquifers are given by relic brines, leaching of gypsum, and dissolution of calcite. The origin of high sulfate concentrations could be either the Late Triassic gypsum beds occurring at approximate depths of 2000 m or evaporites of the Late Tertiary rift brine of the inland sea. For instance, groundwater in Meizar 2 and Hamat Gader has leached different amounts of gypsum/anhydrite and calcite. Ion exchange of Ca^{2+} against Mg^{2+}, Na^+, and K^+ enhanced the concentrations of the latter. Meizar 3 in 2008 resembles Meizar 2 in the same year. Their REY patterns show that this groundwater had dissolved HFO on its altered flow path. The regional distribution of U(VI), Sr^{2+}, and SO_4^{2-} and REY distribution patterns reveal that there is a zone with strongly confined groundwater and the hydrochemical composition changes systematically sideward and downstream along the gorge

(iii) The regional variation of their chemical composition of groundwater is related to a complex flower-structured fault system crossing the gorge. Groundwater flow in the gorge and the mixing between the different water bodies are controlled by these structural features

Data Availability

All underlying data of the research study are included in the manuscript in the form of Tables 1–3.

Conflicts of Interest

The authors declare that they have no conflicts of interest.

Acknowledgments

The research was partly funded by the German Science Foundation (DFG) (grant MA4450/2) and the DESERVE Virtual Institute (VH-VI-527) funded by the Helmholtz-Association of German Research Centers. The authors thank the Mekorot Co. Ltd. and the IDF and JAF for providing access and security during sampling along the international borders.

References

[1] C. Siebert, P. Möller, S. Geyer et al., "Thermal waters in the Lower Yarmouk Gorge and their relation to surrounding aquifers," *Geochemistry*, vol. 74, no. 3, pp. 425–441, 2014.

[2] P. Möller, C. Siebert, S. Geyer et al., "Relationship of brines in the Kinnarot Basin, Jordan-Dead Sea Rift Valley," *Geofluids*, vol. 12, no. 2, 181 pages, 2012.

[3] P. Möller, E. Rosenthal, N. Inbar, and C. Siebert, "Development of the inland sea and its evaporites in the Jordan-Dead Sea Transform based on hydrogeochemical considerations and the geological consequences," *International Journal of Earth Sciences*, vol. 107, no. 7, pp. 2409–2431, 2018.

[4] N. Goretzki, N. Inbar, M. Kühn et al., "Inverse problem to constrain hydraulic and thermal parameters inducing anomalous heat flow in the Lower Yarmouk Gorge," *Energy Procedia*, vol. 97, pp. 419–426, 2016.

[5] F. Magri, N. Inbar, C. Siebert, E. Rosenthal, J. Guttman, and P. Möller, "Transient simulations of large-scale hydrogeological processes causing temperature and salinity anomalies in the Tiberias basin," *Journal of Hydrology*, vol. 520, pp. 342–355, 2015.

[6] F. Magri, S. Möller, N. Inbar et al., "2D and 3D coexisting modes of thermal convection in fractured hydrothermal systems - Implications for transboundary flow in the Lower Yarmouk Gorge," *Marine and Petroleum Geology*, vol. 78, pp. 750–758, 2016.

[7] K. Tzoufka, F. Magri, T. Rödiger et al., "The effect of hydraulic anisotropies on intensely exploited groundwater resources: the numerical evaluation of a hydrothermal transboundary aquifer system in the Middle East," *Hydrogeology Journal*, vol. 26, no. 8, pp. 2875–2890, 2018.

[8] R. Roded, E. Shalev, and D. Katoshevski, "Basal heat-flow and hydrothermal regime at the Golan-Ajloun hydrological basins," *Journal of Hydrology*, vol. 476, pp. 200–211, 2013.

[9] Mekorot, National Water Co, *Records on wells, water levels water quality and exploitation*, Mekorot Company, Tel Aviv, Israel, 1950-2017.

[10] WAJ, *Water Information System Database, accessible via the Ministry of Water and Irrigation*, Jordan Minisitry of Water and Irrigation, Amman, Jordan, 2016, http://www.mwi.gov.jo.

[11] A. Brunner and E. Dekel, "High resolution seismic reflection survey in Southern Golan," Rep.120/1939/88 IPRG–Israel Institute for Petroleum Research and Geophysics, 1989.

[12] M. Meiler, M. Reshef, and H. Shulman, "Seismic depth-domain stratigraphic classification of the Golan Heights, central Dead Sea Fault," *Tectonophysics*, vol. 510, no. 3-4, pp. 354–369, 2011.

[13] J. Sahawneh, "Structural control of hydrology, hydrogeology and hydrochemistry along the eastern escarpment of the Jordan Rift Valley, Jordan," PhD. Thesis, Karlsruher Inst. für Technologie (KIT), 2011.

[14] A. Flexer, "Stratigraphy and facies development of Mt. Scopus Group (Senonian-Paleocene) in Israel and adjacent countries," *Israel Journal of Earth Sciences*, vol. 17, pp. 85–114, 1980.

[15] N. Inbar, E. Rosenthal, F. Magri et al., "Faulting patterns in the Lower Yarmouk Gorge potentially influence groundwater flow paths," *Hydrology and Earth System Sciences*, vol. 23, no. 2, pp. 763–771, 2019.

[16] E. Rosenthal, "Hydrogeology and hydrogeochemistry of the Bet Shean and Harod Valleys," vol. 2, Geol Surv Israel, 1972, Rep. H/2/1972, in Hebrew.

[17] E. Rosenthal, G. Weinberger, A. Almogi-Labin, and A. Flexer, "Late cretaceous-early tertiary development of depositional basins in Samaria (Israel) as part of the evolution of regional folding systems," *AAPG Bulletin*, vol. 84, pp. 997–1042, 1999.

[18] Z. Kattan, "Chemical and environmental isotope study of the fissured basalt aquifer system of the Yarmouk basin," *IAEA Symposium on isotopes in water resources management*, 1995, Vienna, Austria, 1995IAEA-SM/336/28.

[19] E. Dafny, A. Burg, and H. Gvirtzman, "Deduction of groundwater flow regime in a basaltic aquifer using geochemical and isotopic data: the Golan Heights, Israel case study," *Journal of Hydrology*, vol. 330, no. 3-4, pp. 506–524, 2006.

[20] T. Rödiger, S. Geyer, U. Mallast et al., "Multi-response calibration of a conceptual hydrological model in the semiarid catchment of Wadi al Arab, Jordan," *Journal of Hydrology*, vol. 509, pp. 193–206, 2014.

[21] E. Salameh, "Using environmental isotopes in the study of recharge-discharge mechanisms of the Yarmouk catchment area in Jordan," *Hydrogeology Journal*, vol. 12, pp. 451–463, 2004.

[22] K. Schelkes, *Groundwater balance of the Jordan-Syrian basalt aquifer*, BGR Bundesanstalt für Geowissenschaften und Rohstoffe, Hannover, 1997.

[23] UN-ESCWA and BGR (United Nations Economic and Social Commission for Western Asia and Bundesanstalt für Geowissenschaften und Rohstoffe), *Inventory of shared water resources in Western Asia. Chapter 21*, Yarmouk Basin Basalt Aquifer System, 2013.

[24] W. Wagner, *Groundwater in the Arab Middle East*, Springer-Verlag, Berlin, Heidelberg, 2011.

[25] A. Sneh, Y. Bartov, T. Weissbrod, and M. Rosensaft, *Geological map of Israel 1:2200,000. Israel Geological Survey (4 Sheets)*, Geological Survey of Israel, Jerusalem, Israel, 1998.

[26] G. Brew, M. Barazangi, A. K. Al-Maleh, and T. Sawaf, "Tectonic and geologic evolution of Syria," *GeoArabia*, vol. 6, no. 4, pp. 573–616, 2001.

[27] R. Wolfart, "Hydrogeology of the Damascus basin (Southwest-Syria)," *IAHS Red Books*, vol. 64, pp. 402–413, 1964.

[28] E. Dafny, H. Gvirtzman, A. Burg, and L. Fleischerc, "The hydrogeology of the Golan basalt aquifer, Israel," *Israel Journal of Earth Sciences*, vol. 52, no. 3-4, pp. 139–153, 2003.

[29] H. Michelson, "The hydrogeology of the southern Golan Heights," Tahal, Tel Aviv. Rep, 1972, HR/72/037.

[30] H. Michelson, "The geology and paleogeography of the Golan Heights," Tel Aviv University, Tel Aviv. PhD thesis, 1979.

[31] P. Möller, E. Rosenthal, N. Inbar, and F. Magri, "Hydrochemical considerations for identifying water from basaltic aquifers: the Israeli experience," *Journal of Hydrology: Regional Studies*, vol. 5, pp. 33–47, 2016.

[32] A. Heimann, "The Dead Sea rift and its margins. Development of Northern Israel in the Pliocene and Pleistocene," PhD Thesis Hebrew Univ, 1990.

[33] D. Mor, "The volcanism of the Golan Heights," Geol Surv Isr, 1986, Rep.GSI/5/86.

[34] B. K. Moh'd, *The geology of Irbid and Ash Shuna Ash Shamaliyya (Waqqas) Map Amman, Sheets No. 3154-II and 3154-III*, Natural Resources Authority, Geology Directorate, Amman, Jordan, 2000.

[35] M. Tichomirowa, C. Heidel, M. Junghans, F. Haubrich, and J. Matschullat, "Sulfate and strontium water source identification by O, S and Sr isotopes and their temporal changes (1997-2008) in the region of Freiberg, central-eastern Germany," *Chemical Geology*, vol. 276, no. 1-2, pp. 104–118, 2010.

[36] P. Möller, E. Rosenthal, P. Dulski, and S. Geyer, "Characterization of recharge areas by rare earth elements and stable isotopes of H_2O," in *The Water of the Jordan Valley*, H. Hötzl, P. Möller, and E. Rosenthal, Eds., pp. 123–148, Springer Verlag, Berlin, Heidelberg, 2009.

[37] C. Siebert, E. Rosenthal, P. Möller, T. Rödiger, and M. Meiler, "The hydrochemical identification of groundwater flowing to the Bet She'an- Harod multiaquifer system (Lower Jordan Valley) by rare earth elements, yttrium, stable isotopes (H, O) and Tritium," *Applied Geochemistry*, vol. 27, no. 3, pp. 703–714, 2012.

[38] G. Bergelson, R. Nativ, and A. Bein, "Salinization and dilution history of ground water discharging into the Sea of Galilee, the Dead Sea Transform, Israel," *Applied Geochemistry*, vol. 14, no. 1, pp. 91–118, 1999.

[39] O. Klein-BenDavid, E. Sass, and A. Katz, "The evolution of marine evaporitic brines in inland basins: The Jordan-Dead Sea Rift valley," *Geochimica et Cosmochimica Acta*, vol. 68, no. 8, pp. 1763–1775, 2004.

[40] G. E. Brown Jr., T. P. Trainor, and A. M. Chaka, "Geochemistry of mineral surfaces and factors affecting their chemical reactivity," in *Chemical Bonding at Surfaces and Interfaces*, A. Nilsson, P. LGM, and J. Norskov, Eds., pp. 457–509, Elsevier, New York, 2008.

[41] E. S. Larsen and D. Gottfried, *Distribution of uranium in rocks and minerals of Mesozoic batholith in Western United States*, vol. 1070-C, US Geol Surv Bull, 1961.

[42] T. A. Marshall, K. Morris, G. T. W. Law et al., "Incorporation of uranium into hematite during crystallization from ferrihydrite," *Environmental Science & Technology*, vol. 48, no. 7, pp. 3724–3731, 2014.

[43] H. E. Roberts, K. Morris, G. T. W. Law et al., "Uranium(V) incorporation mechanisms and stability in Fe(II)/Fe(III) (oxyhydr)oxides," *Environmental Science & Technology Letters*, vol. 4, no. 10, pp. 421–426, 2017.

[44] M. R. Romero-González, T. Cheng, M. O. Barnett, and E. E. Roden, "Surface complexation modeling of the effects of phosphate on uranium(VI) adsorption," *Radiochimica Acta*, vol. 95, no. 5, 2007.

[45] G. N. Baturin and A. V. Kochenov, "Uranium in Phosphorites," *Lithology and Mineral Resources*, vol. 36, no. 4, pp. 303–321, 2001.

[46] V. S. Tripathi, "Comments on "Uranium solution-mineral equilibria at low temperatures with applications to sedimentary ore deposits"," *Geochimica et Cosmochimica Acta*, vol. 43, no. 12, pp. 1989-1990, 1979.

[47] S. Göb, T. Wenzel, M. Bau, D. E. Jacob, A. Loges, and G. Markl, "The redistribution of rare-earth elements in secondary minerals of hydrothermal veins, Schwarzwald, SOUTHWESTERN Germany," *The Canadian Mineralogist*, vol. 49, no. 5, pp. 1305–1333, 2012.

[48] P. Möller and C. Siebert, "Cycling of calcite and hydrous metal oxides and chemical changes of major element and REE chemistry in monomictic hardwater lake: impact on sedimentation," *Chemie der Erde*, vol. 76, no. 1, pp. 133–148, 2016.

[49] M. Raab, G. M. Friedman, B. Spiro, A. Starinsky, and I. Zak, "The geological history of Pliocene-Pleistocene evaporites in Mount Sedom (Israel) and how strontium and sulfur isotopes relate to their origin," *Carbonates and Evaporites*, vol. 15, no. 2, pp. 93–114, 2000.

[50] W. B. F. Ryan, "Modeling the magnitude and timing of evaporative drawdown during the Messinian crisis," *Stratigraphy*, vol. 5, pp. 227–243, 2008.

[51] A. E. Shimron, "Geochemical exploration and new geological data along the SE flanks of the Hermon Range," Geol Surv Isr, Jerusalem, 1989, Rep GSI/32/89.

[52] H. Brielmann, "Recharge and discharge mechanism and dynamics in the mountainous northern upper Jordan River catchment, Israel," Ph.D. thesis LMU, Munich, Germany, 2008.

[53] A. R. Al Charideh and B. A. Zakhem, "Distribution of tritium and stable isotopes in precipitation in Syria," *Hydrological Sciences Journal*, vol. 55, no. 5, pp. 832–843, 2010.